Materials Advances

ROYAL SOCIETY OF CHEMISTRY

REVIEW

View Article Online
View Journal | View Issue

Cite this: *Mater. Adv.*, 2020, **1**, 119

Earth abundant colloidal carbon quantum dots for luminescent solar concentrators

Guiju Liu,†[ab] Xiaohan Wang,†[ac] Guangting Han,*[a] Jianyong Yu*[d] and Haiguang Zhao *[ab]

Luminescent solar concentrators (LSCs) can serve as large-area sunlight collectors, suitable for applications in low-cost optoelectronic devices. The external optical efficiency of LSCs is significantly dependent on the optical properties of the chosen fluorophores. Compared to organic dyes/polymers and inorganic nanocrystals, carbon quantum dots (C-dots) have emerged as a new class of fluorophores in LSCs due to their tunable absorption spectrum, high quantum yield, non-toxicity, environmental friendliness, low-cost and eco-friendly synthetic methods. Major discoveries have been made in this field very recently, while there is a lack of an up-to-date systematic review to summarize the employment of C-dots in LSCs. In this review, we summarized the most recent advances in this field, focusing on the structure-dependent optical properties of C-dots for LSCs. We review various synthetic strategies developed for the synthesis of high-quality C-dots using green precursors and solvents, yielding C-dots with a wide absorption spectrum, large Stokes shift and high quantum yield. We further discuss in detail the relationship between the structure and optical properties of C-dots. We conclude with a detailed account of the latest examples of C-dot applications in the structure and performance of LSCs and give our own perspectives on the remaining key issues and emerging possibilities in the field.

Received 8th April 2020,
Accepted 26th April 2020

DOI: 10.1039/d0ma00181c

rsc.li/materials-advances

[a] *State Key Laboratory of Bio-Fibers and Eco-Textiles, Qingdao University, No. 308 Ningxia Road, Qingdao 266071, P. R. China. E-mail: kychgt@qdu.edu.cn, hgzhao@qdu.edu.cn*

[b] *College of Physics, University Industry Joint Center for Ocean Observation and Broadband Communication, Qingdao University, No. 308 Ningxia Road, Qingdao 266071, P. R. China*

[c] *College of Textiles & Clothing, Qingdao University, No. 308 Ningxia Road, Qingdao 266071, P. R. China*

[d] *Innovation Center for Textile Science and Technology, Donghua University, No. 1882 West Yan An Road, Shanghai, 200051, P. R. China. E-mail: yujy@dhu.edu.cn*

† These authors contributed equally to this work.

1. Introduction

Converting solar energy to electricity and fuels represents a promising opportunity towards addressing the increasing demand for clean and renewable energy.[1–17] Compared to traditional fossil fuels, the use of solar energy can reduce carbon emissions which lead to environmental pollution and climate change.[1–5] Silicon solar cells have been widely used for solar-to-electricity conversion with high power conversion

Guiju Liu

Guiju Liu received her Bachelor degree in Materials Physics from Qingdao University (China) in 2014. She obtained her Master degree at Qingdao University (China) in 2017. Currently, she is a PhD student majoring in Materials Physics and Chemistry at Qingdao University. Her research mainly focuses on the synthesis and structural characterization of quantum dots and their applications in luminescent solar concentrators and hydrogen generation.

Xiaohan Wang

Xiaohan Wang is presently a PhD candidate under the supervision of Prof. Guangting Han and Prof. Jianyong Yu at Qingdao University, China. She received her BS degree in 2013 and MS degree in 2016 from Qingdao University. Her current research interests mainly focus on electrospun fiber derived functional materials and quantum dots.

efficiency (PCE) and long-term stability.[4,5] However, the cost of electricity generated by silicon solar cells is still much higher than that generated by fossil fuels, or hydro/wind-electricity. Researchers have fabricated the third-generation excitonic solar cells [*e.g.* quantum dot (QD) solar cells, perovskite solar cells, and dye solar cells].[18–24] However the PCE and long-term stability of excitonic solar cells still have a lot of room to improve. During the last forty years, luminescent solar concentrator (LSC) technology has attracted a lot of attention as a solar-light harvester, which can significantly reduce the cost of electricity by decreasing the active area of silicon solar cells used for generating the same amount of power, if the PCE of the LSCs is higher than 6%.[25–29] In addition, LSCs could be very suitable for application in building-integrated photovoltaic (BIPV) applications due to their transparent or semi-transparent nature, light weight, and low-light intensity photovoltaic (PV) response.[30,31]

An LSC typically consists of a plastic optical waveguide doped with highly emissive fluorophores (*e.g.* dyes, polymers, and QDs).[32] The working principle and energy loss mechanisms are shown in Fig. 1. After absorbing sunlight, the fluorophores emit photons and these photons are guided towards the PV devices placed at the LSC edges by total internal reflection (TIR). The PV devices can convert the concentrated fluorescence to electricity. The theoretical external optical efficiency (η_{opt}) of an LSC is defined as the photons emitted from the LSC edges over the total photons impinging on the LSC through the top surface. It can be calculated as:[32]

$$\eta_{opt} = (1 - R)\eta_{TIR}\cdot\eta_{abs}\cdot\eta_{QY}\cdot\eta_{Stokes}\cdot\eta_{host}\cdot\eta_{self}$$

where R is the reflection of solar light from the waveguide surface (number 1), η_{TIR} is the TIR efficiency (number 2), η_{abs} is the fraction of solar light that is absorbed by the fluorophores (number 3), η_{QY} is the fluorescent quantum yield (QY) of the fluorophores (number 4), η_{Stokes} is the energy loss due to heat generation during the absorption and emission event, η_{host} is the transport efficiency of the wave-guided photons through the waveguide, and η_{self} is related to re-absorption of the emitted photons by another fluorophore in the waveguide (number 5). The key to obtain high-efficiency LSCs is to design and synthesize high quality fluorophores with broad absorption, matching well with the Sun's spectrum, high QY, large Stokes shift

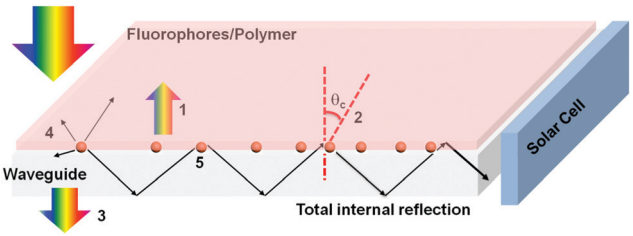

Fig. 1 Schematic representation of a typical LSC. The numbers indicate the typical processes of energy loss in an LSC. (1) Reflected light from the top surface; (2) emission escapes from the surface due to the escape cone; (3) unabsorbed light; (4) partial energy loss due to the non-unity of the QY; and (5) light is reabsorbed by another fluorophore.

Guangting Han

Guangting Han is a Professor of College of Textiles & Clothing and Director of State Key Laboratory of Bio-Fibers and Eco-Textiles, Qingdao University. He received his Master degree (1988) from China Textile University and PhD degree (2006) from Donghua University. His research interests focus on the structure and performance of textile fiber materials, new textile materials, new processes and equipment, and comprehensive development and utilization of environmentally friendly polymer materials.

Jianyong Yu

Prof. Jianyong Yu received his BS, MS and PhD degrees from the College of Textiles at Donghua University in 1985, 1988 and 1991, respectively. He is currently a Full Professor at Innovation Center for Textile Science and Technology at Donghua University and an academician of the Chinese Academy of Engineering. His research interests include natural and synthetic fibers, functional textile materials, textile composites, industrial textiles etc.

Haiguang Zhao

Haiguang Zhao received his BS degree (2005) from University of Jinan, MSc degree (2007) from Zhejiang University and PhD degree in Energy and Materials Science (2012) from INRS, Quebec University. Currently he is a full professor at the State Key Laboratory and College of Physics, Qingdao University, since February 2018. His research interests focus on the synthesis of semiconductor materials (including metal oxides, quantum dots and perovskites) and nanofibers for optoelectronic applications, such as solar cells, luminescent solar concentrators, thermal sensors, and solar-driven water splitting. He is a Member of the Global Young.

(small overlap between the absorption and emission spectra of the fluorophores), high absorption coefficient and good stability.[25,27,30,33–35] In the past forty years of research, various types of fluorophores have been used as absorbers/emitters for LSCs, including organic dyes, polymers, upconversion nanocrystals (NCs), quantum wells, QDs and perovskite NCs *etc.*[8,27,33,36–40] Among them, colloidal QDs have attracted a lot of attention as fluorophores for application in LSCs due to their excellent optical properties, including size/shape/chemical composition tunable absorption spectra, structurally engineered Stokes shift, high QYs and improved photostability compared to traditional organic dyes/polymers.[8,29,38,40–43] However, most inorganic QDs (*e.g.* PbS/CdS, CdSe/CdS, and CuInSe/ZnS) are very sensitive to oxygen and moisture during the synthesis, purification and LSC preparation process,[8,38,44–47] and some QDs contain toxic elements (*e.g.* Cd and Pb),[48–51] environmentally sensitive elements (*e.g.* Se and S),[38,47] or non-earth-abundant and expensive metals (*e.g.* In and Ag).[38,47,52]

Among various types of QDs, carbon QDs (C-dots) have attracted a lot of attention owing to their unique optical properties for various kinds of potential applications, such as bio-imaging, bio-markers, thermal sensors, light emitting devices and energy converting devices. C-dots are semiconductors with a size of less than 10 nm. For those carbon nanoparticles without crystal structure, they have a molecule-like behavior, and do not have size-dependent optical properties. Therefore, this type of carbon nanoparticles does not belong to the family of QDs. Most C-dots are composed of non-toxic and earth-abundant elements (C, N and O) and can be synthesized in large quantities *via* simple, low-cost and eco-friendly wet-chemical approaches using sustainable, low-cost precursors and relatively non-toxic solvents. They have size/shape/chemical composition tunable absorption/emission spectra, high QY and high colloidal-, thermal- and photostability. Very recently, great efforts have been made in using C-dots as efficient fluorophores for LSC applications. Although several recent reviews have described advances in LSCs, focusing on the different types of fluorophores (dyes, polymers, and QDs), waveguide materials and configuration of LSCs, there is still no report focusing on the use of C-dots for efficient LSCs.[16,25,27,30,31,33–35,43,53]

Our objective in this review is to highlight recent developments and exciting perspectives in the field of C-dots in terms of their synthesis, optical properties, and their applications in LSCs. Specifically, we present the key aspects of the design and synthesis of crystalline C-dots through different methods and the control of the optical properties of C-dots by tuning their size/shape, chemical composition and surface chemicals, and review emerging applications of LSCs. We focus on the correlations between the structure and optical properties of C-dots and improving the optical efficiency of LSCs through the selection of C-dots and the LSC configuration.

2. Synthesis and structure of C-dots

The optical properties of C-dots are highly dependent on their structure.[18,54–84] The development of simple, efficient synthetic routes for high-performance C-dots with respect to well controlled size/shape and chemical composition is crucial to exploit the relationship between their structure and optical properties.[18,54–84] In this section, we summarized various reported methods to produce colloidal C-dots. We mainly focus on the production of C-dots in large quantity using low-cost, sustainable precursors and solution-based synthetic routes include hydro-/solvothermal synthesis, pyrolysis carbonization synthesis, microwave-assisted synthesis and electrochemical synthesis. These approaches are very powerful for the reproducible synthesis of C-dots because they allow controlling the structure and optical properties of the materials.

2.1 Hydro-/solvothermal synthesis of C-dots

The hydro/solvothermal method has been considered as a facile way to synthesize C-dots from carbon-containing precursors (*e.g.* sugar compounds, organics, and biomass materials), benefiting from their advantages, such as low cost, eco-friendly nature and ease of handling.[57,83] Typically, the carbon-containing precursors were mixed with water or organic solvents and then the mixture was transferred into a Teflon-lined autoclave for high temperature (100–250 °C) reaction to obtain C-dots.[85] The structure and optical properties of the C-dots can be adjusted by tuning the reaction conditions, including the type of precursors, solvents, reaction time, reaction temperature, *etc.* For example, Qu *et al.* prepared orange emissive fluorescent C-dots with average sizes ranging from 4 to 10 nm *via* a solvothermal route using citric acid (CA) and urea as precursors and dimethylformamide (DMF) as a solvent.[86] Zboril *et al.* prepared C-dots *via* a solvothermal method by dissolving CA and urea in formamide (Fig. 2a).[87] The post-size selection by silica column chromatography can well separate the C-dots with sizes from 2 to 3 nm (Fig. 2b–e). The C-dots have size dependent emission, indicating a strong quantum confinement in these C-dots.

Fan *et al.* reported the synthesis of C-dots *via* a solvothermal reaction using phloroglucinol triangulogen as a precursor and ethanol or DMF as a solvent.[88] In the synthesis, with the addition of a catalyst (HCl or H_2SO_4), larger sized C-dots can be obtained compared to the reaction system without adding the catalyst. The as-prepared C-dots have a typical triangular shape and the size can be well controlled by tuning the reaction time (Fig. 3b–e). The as-prepared C-dots have a broad size distribution (1.9 nm to 3.9 nm). With further purification by silica column chromatography, the as-prepared C-dots can be further size-selected. As shown in Fig. 3b–e, a defect-free graphene crystalline structure with an obvious triangular shape was found in the TEM images of the C-dots. Recently, there were numerous reports of the synthesis of C-dots using natural biomass as a carbon source, including orange juice,[84] lemon juice,[61,89] rice residue[76] *etc.* The controllable synthesis of C-dots using precursors derived from sustainable biomass by the hydrothermal process is a facile, eco-friendly and economical way.[55,59,76,90–92]

2.2 Pyrolysis carbonization synthesis of C-dots

Pyrolysis is a reaction process to synthesize C-dots using a carbon source that is decomposed by heat. Compared to liquid-phase

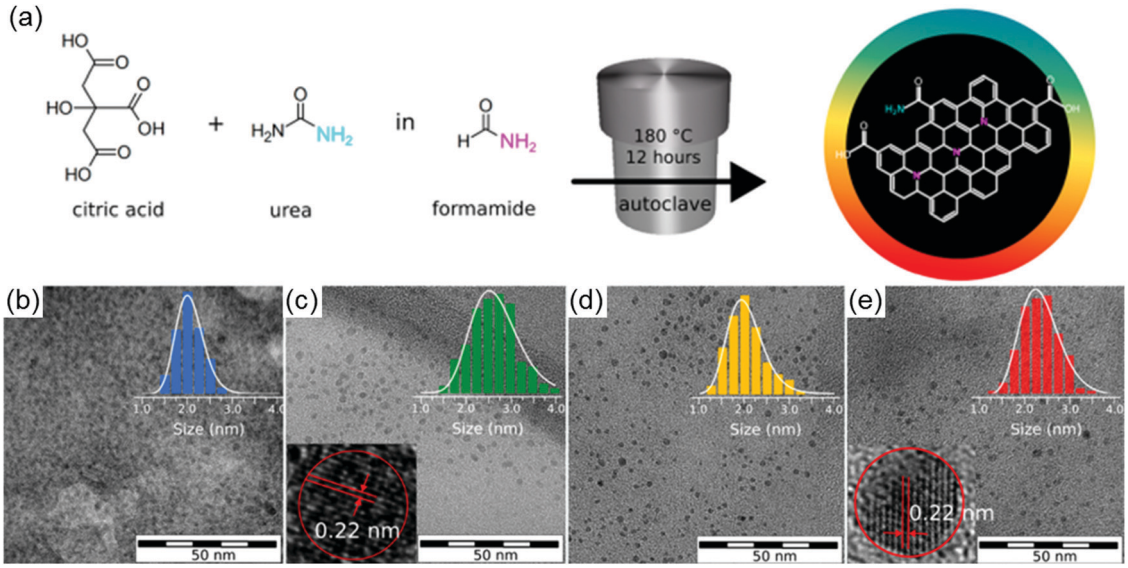

Fig. 2 (a) Reaction scheme used for the preparation of mixture-dots *via* a solvothermal reaction. Transmission electron microscopy (TEM) and diameter histogram of the separated fractions of C-dots with (b) blue color, (c) green color, (d) yellow color and (e) red color. The insets of figure (c) and (e) are the high resolution TEM of the green and red color C-dots. Reproduced with permission from ref. 87. Copyright 2017, American Chemical Society.

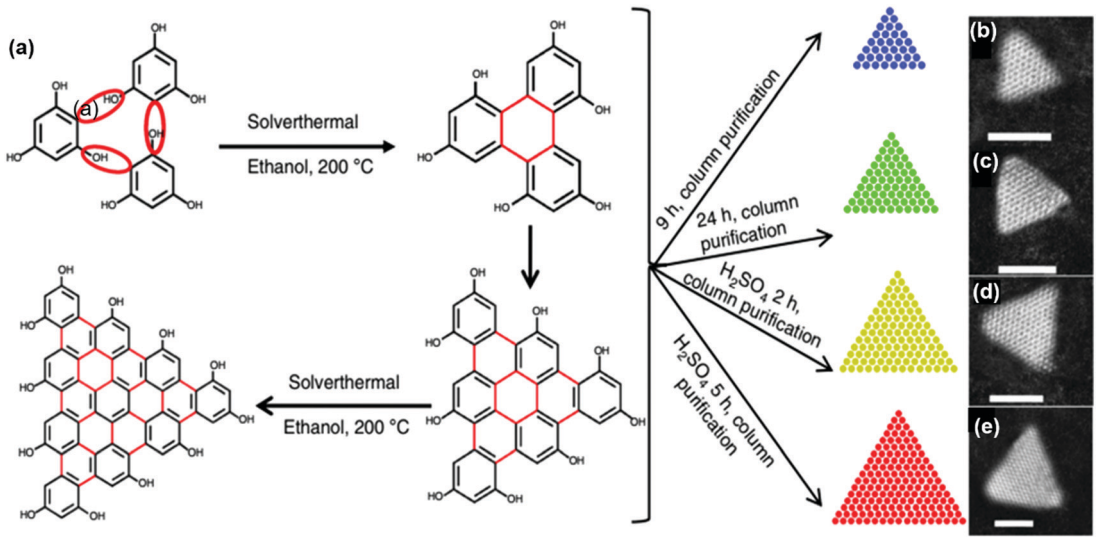

Fig. 3 (a) Synthesis route of the C-dots using a solvothermal reaction. The typical aberration-corrected high-angle annular dark-field scanning TEM (HAADF-STEM) images of the as-synthesized C-dots with blue (b), green (c), yellow (d), and (e) red colors by tuning the reaction conditions. The scale bar is 2 nm. Reproduced with permission from ref. 88. Copyright 2018, Springer Nature.

reactions (*e.g.* hydrothermal or solvothermal), there is no solvent in the pyrolysis reaction.[56,76,93–95] Many precursors from biomass have been used to produce C-dots *via* pyrolysis reactions.[56,76,93–95] For instance, Martindale's group reported the synthesis of C-dots by pyrolyzing CA at 180 °C with a yield of 45% and a size of 6.8 ± 2.3 nm.[93] Wang *et al.* reported the large-scale and controllable synthesis of C-dots with a yield of 15% from rice husk.[76] Similar to liquid-phase reactions, the pyrolysis reaction also leads to a wide size distribution of C-dots.[93] Very recently, Zhou *et al.* reported the synthesis of C-dots with a very narrow size distribution *via* a space-confined vacuum heating approach.[96] In a typical synthesis, a mixture of CA, urea and $CaCl_2$ was dissolved in water. The mixture was heated to 120 °C in order to form an inflated foam. With the temperature increased further, uniform C-dots were formed through dehydration and carbonization processes taking place in the confined spaces of the thin foam walls (Fig. 4a). The prepared C-dots after purification have a uniform average particle diameter of 4.1 nm and graphitic carbon structure (Fig. 4b). An X-ray powder diffraction (XRD) pattern of the C-dots film showed a diffraction peak centered at 3.2 Å (Fig. 4c). Based on the Fourier transform infrared spectroscopy (FT-IR) measurement, purification using a dialysis tube can separate well the precursors

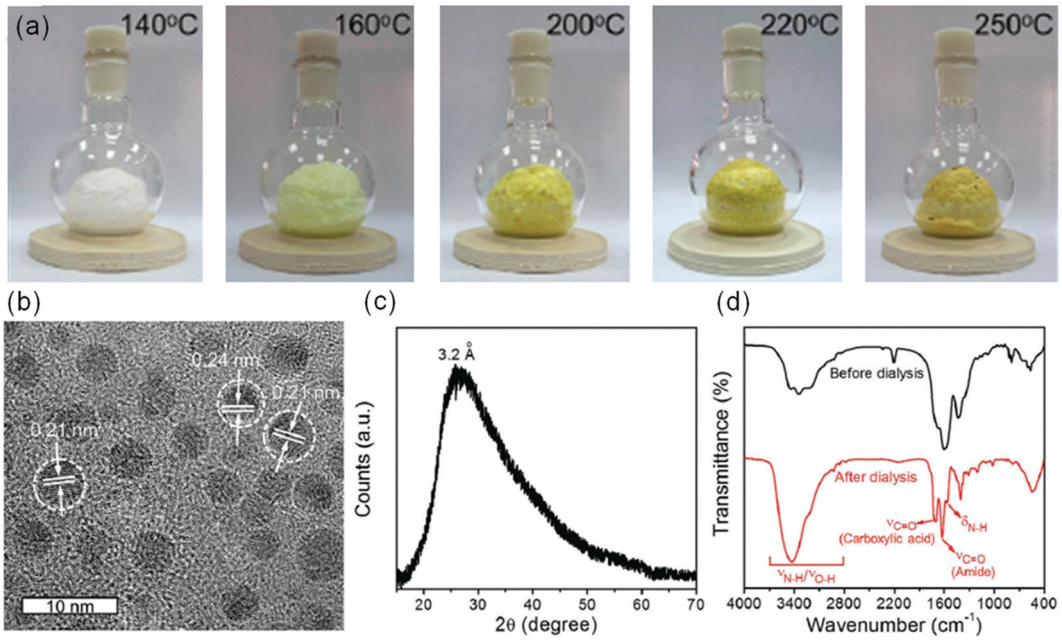

Fig. 4 (a) Photographs of the inflated foams prepared by the vacuum heating method at different temperatures, taken under sunlight. (b) HRTEM image of the C-dots synthesized by the vacuum heating method at 250 °C. (c) XRD pattern, and (d) FT-IR spectra of C-dots before (black line) and after (red line) purification. Reproduced with permission from ref. 96. Copyright 2019, Royal Society of Chemistry.

from the C-dots (Fig. 4d). Due to the highly narrow size distribution and good surface passivation, the C-dots have a very high QY (60–70%) in both the liquid phase and solid phase, while this approach can only produce green C-dots.[96] Further research should be focused on the production of C-dots with various colors using the space-confined vacuum heating approach.

2.3 Microwave synthesis of C-dots

Compared to the above-mentioned heating methods, microwaves can provide efficient and rapid localized heating because of the strong interaction between the carbon precursors and the microwaves. This approach can provide large-scale C-dots with reduced reaction time compared to other methods. There have been many reports for the preparation of C-dots using microwave methods.[77,97] Wang *et al.* prepared C-dots from wool *via* a microwave method.[77] The obtained C-dots have a QY of 16.3% with a size range of 1.5–4.5 nm. Yao's group synthesized Gd^{3+}, Mn^{2+} and Eu^{3+} doped C-dots *via* microwave synthesis using crab shell as the starting materials (Fig. 5a).[98] Chitin derived from crab shell acted not only as a carbon source but also as a chelating ligand to form complexes with transition-metal ions. Si *et al.* reported a microwave-assisted strategy toward the synchronous preparation of nitrogen-doped C-dots within 10 min.[99] The prepared C-dots have a size ranging from 2 nm to 3 nm. Jiang *et al.* synthesized C-dots on the gram scale by microwave-assisted carbonization of ethanolamine and phosphoric acid aqueous solution (Fig. 5b).[69] They can produce C-dots of ~2.8 g in one batch reaction within 5 min (750 W). This approach is very efficient for further potential applications of C-dots in LSCs because we need a large amount of C-dots for fabrication of LSCs.

2.4 Electrochemical synthesis of C-dots

C-dots can also be produced by the electrochemical method. Usually the size and structure of C-dots can be controlled by tuning the type of electrolyte and applied voltage. The obtained C-dots have several advantages, such as relatively high purity, high product yield, low cost, easy control over the size and chemical composition, and good repeatability.[62,81,100] Deng *et al.* prepared C-dots directly from low-molecular-weight alcohols *via* the electrochemical method.[81] The size of the as-prepared C-dots can be adjusted by varying the applied potential. Without further complicated purification and passivation procedures, the obtained C-dots exhibited a QY of 15.9%. Very recently, He *et al.* reported an electrochemical exfoliation method to synthesize C-dots with a size of 3.02–4.61 nm by using a cut piece of commercial coke directly as the working electrode.[101] Compared with other synthesis methods of C-dots, the electrochemical method does not require further complicated purification procedures,[101] while the as-prepared C-dots have a lower QY than that of those synthesized by other approaches.[62,81,100,101]

We summarized the synthesis of C-dots using different precursors and solvents through the above-mentioned methods. The hydro/solvothermal method is very simple to operate and the properties of the C-dots can be well controlled by controlling the degree of decomposition. The pyrolysis method is also easy to operate and the system can be solvent free. The advantage of the microwave method is that one could obtain a large quantity of C-dots with short reaction time. However, the size of the C-dots synthesized by these methods is not very uniform and usually requires further complicated purification procedures. The electrochemical method has a relatively high utilization rate of carbon sources, and does not require further separation and purification

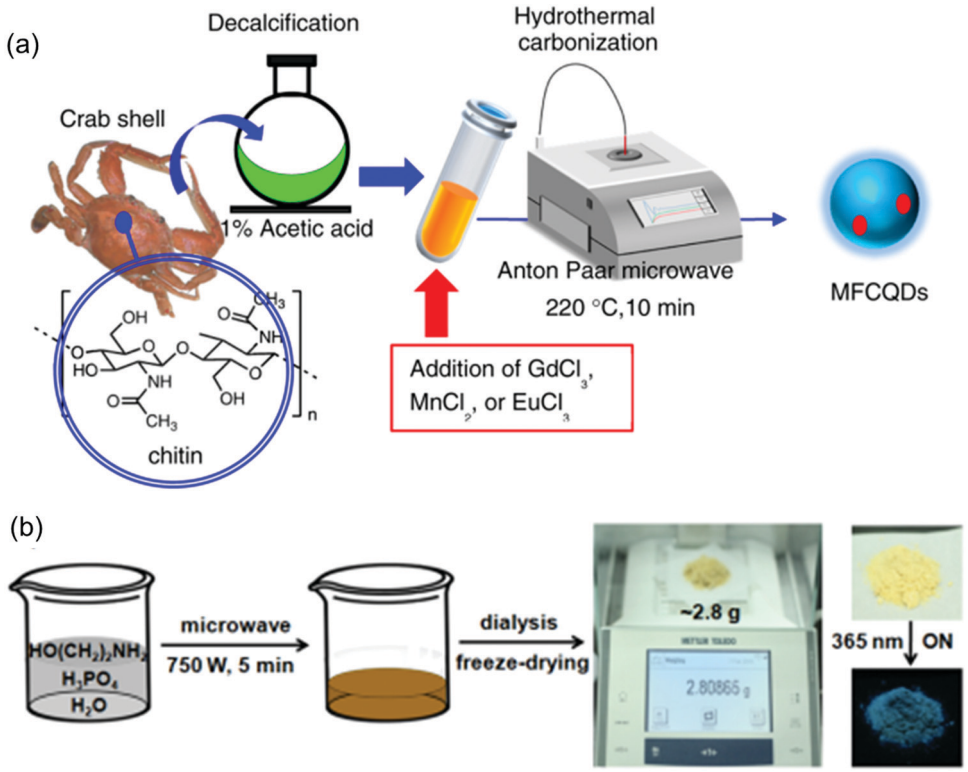

Fig. 5 (a) Schematic illustration of preparation of C-dots by a microwave-assisted approach. (b) Schematic illustration of the preparation process for C-dots with a gram scale product. Right side of (b): the purified C-dot powder under daylight and a 365 nm ultraviolet (UV) lamp. (a) Reproduced with permission from ref. 98. Copyright 2017, American Chemical Society. (b) Reproduced with permission from ref. 69. Copyright 2018, Wiley-VCH.

processes, but the optical properties of C-dots are not so excellent compared to the C-dots synthesized *via* other methods. Further research directions should focus on the large-scale production of C-dots with high optical properties and narrow size distribution using relatively eco-friendly precursors and solvents, such as CA and water. In addition, it is very important to find an efficient and rapid way to purify the as-prepared C-dots, as currently the purification process is very complicated and time-consuming, involving a post purification process using silica column chromatography or dialysis.[96,102]

3. Exciton dynamics and optical properties of C-dots

To fabricate large-area, high-efficiency LSCs, the C-dots are required to have a broad absorption spectrum, large Stokes shift, high QY and good stability.[30] The current obtained C-dots have very unique optical properties, including size tunable absorption/emission spectra covering from 300 to 1000 nm, structure and surface dependent Stokes shift, high QY up to 99% and very good colloidal-, thermal- and photo-stability, which open a new avenue as building blocks for LSC fabrication.[74,103–107]

3.1 Exciton dynamics in C-dots

There are two popular photoluminescence (PL) models to explain the PL mechanism of C-dots: one is based on the band gap transitions in conjugated π-domains, and the other is related to surface energy states on the C-dots.[67,70,88,108,109] For the first one, the band energy gap of C-dots is strongly dependent on the size of the C-dots, a similar behavior to inorganic QDs.[88] Typically, the C-dots have excitation-independent PL characteristics.[70,88] For the latter, the PL is dominated by the surface energy states (surface "molecular states" or trap/defect states).[67,109] Usually these energy states are very sensitive to the surrounding environment (*e.g.* pH, light, and heat).[67,109] The C-dots have excitation-dependent emission characteristics.[67] Table 1 summarizes the PL mechanism of various types of C-dots. Ding *et al.* reported the synthesis of C-dots with tunable colors using a hydrothermal reaction (Fig. 6a).[108] All C-dot samples have similar sizes, which excludes the possibility of size-dependent energy transitions. The authors found that the surface of the C-dots is composed of conjugated carbon atoms and bonded oxygen atoms.[108] They proposed that the C-dots have a core and amorphous molecule-like shell (Fig. 6b). The band gap of the core/shell structure between the highest occupied molecular orbital (HOMO) and the lowest unoccupied molecular orbital (LUMO) is strongly dependent on the incorporated oxygen species (Fig. 6a and b).[108] A PL red shift could arise as a result of an increase in the degree of surface oxidation. As shown in Fig. 6c–f, the PL peaks of the C-dot samples did not shift when different excitation wavelengths were applied. This behavior is very different to other C-dots that have excitation-dependent emission, in which the PL peak

Table 1 Emission mechanisms of various types of C-dots synthesized *via* different methods

C-dot types	Preparation methods	Emission mechanism	Ref.
Multi-color emissive C-dots	Thermal pyrolysis method	Excitation-dependent emission: surface functional groups, effective conjugation length	67
Full-color light-emitting C-dots	One-pot hydrothermal synthesis and purification by gel chromatography	Excitation-dependent emission: surface oxidation	108
Full-color C-dots	Refluxing of chloroform and diethylamine	Excitation-dependent emission: fluorescent molecules on the surface and emissive graphitic fragments in the core	110
Multi-color emissive C-dots	Solvothermal method with $(NH_4)_2CO_3$	Excitation-dependent emission: surface functional groups, multi-emission domains on the surface	111
Green and red emissive switching C-dots	Solvothermal method and separation by silica gel column chromatography	Excitation-dependent emission: surface electron state	109
Blue C-dots, green C-dots	Hydrothermal and separation by size-exclusion chromatography	Excitation-independent emission: π-conjugated electron structure, surface state and groups	112
C-dots	One-pot solvothermal route	Excitation-independent emission: surface states, particle size, sp^2-conjugated domains and the graphitic nitrogen content	70
Narrow bandwidth emission triangular C-dots	Solvothermal method	Excitation-independent emission: band-edge exciton-state decay, direct exciton recombination	88
Red-emissive N-doped C-dots	One-pot solvothermal reaction	Excitation-independent emission: N-related surface defect states	113
C-dots	Hydrothermal method	Excitation-independent emission: surface oxidation and particle size	114
Polymer C-dots	Hydrothermal method	150 °C: excitation-independent emission: molecule state emission or crosslink-enhanced emission 200 °C: synergistic effect of the carbon core and the surface state 250 °C: excitation-dependent emission: carbogenic cores	115

positions shift with the variation of excitation.[3,86] Yuan *et al.* reported the synthesis of C-dots capped with $-NO_2$ through a solvothermal reaction using 3,4,9,10-nitroperylene as a precursor.[109] The color of the C-dots can be adjusted by controlling their surface electronic states with the addition of an alkali.[109] The phenomenon has been ascribed to the presence of multiple luminescent centers in C-dots, or a mixture of various luminescent substances (*e.g.* "molecular states"),[109] while it is still a challenge to directly observe the core/shell structure in C-dots and further investigation should be focused on deep study of the PL mechanism by investigating both the structure and e–h dynamics of C-dots by transient PL spectroscopy and pump–probe measurements.

3.2 Absorption/photoluminescence spectra in C-dots

In the LSC system, the C-dots should have the capability to absorb sunlight, and thus the absorption spectrum of the C-dots should match with the Sun's spectrum.[116,117] C-dots have excellent absorption properties.[116,117] Hereafter, we denote the C-dots with an absorption range of 300–400 nm as UV C-dots, C-dots with an absorption range of 300–700 nm as visible C-dots and C-dots with an absorption spectrum in the

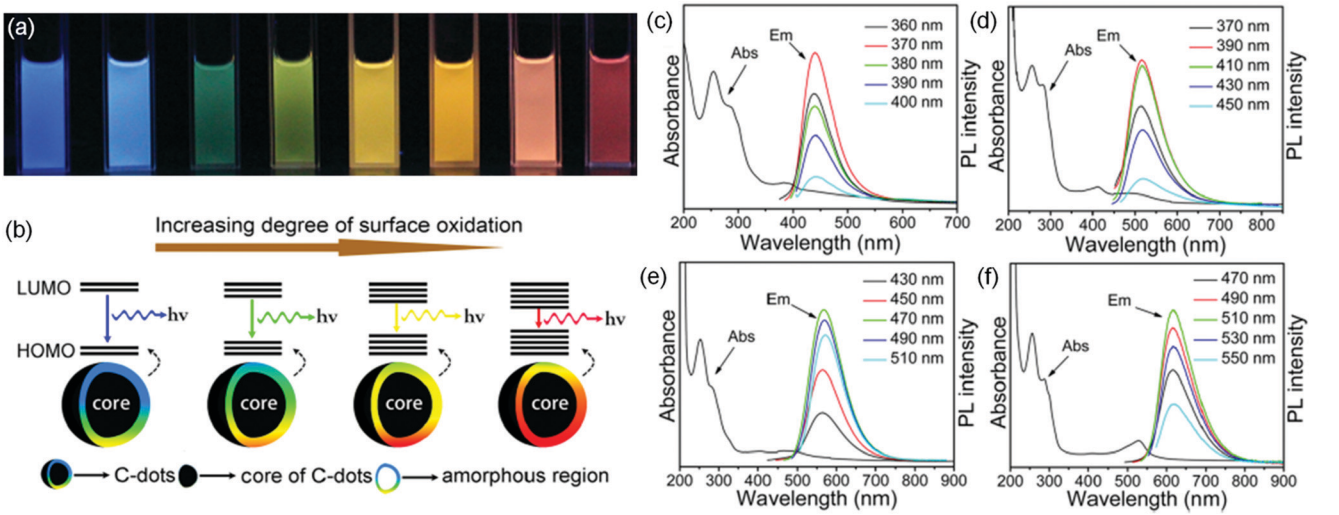

Fig. 6 (a) Photographs of C-dots with tunable colors under UV illumination. (b) Model of the tunable PL of C-dots with different degrees of oxidation. (c–f) The absorption curves (Abs) and PL spectra (Em) of different C-dots under different excitation wavelengths. Reproduced with permission from ref. 108. Copyright 2016, American Chemical Society.

UV-visible-near infrared (NIR) range (300–1400 nm) as NIR C-dots. Boron-and-nitrogen co-doped C-dots (BN-C-dots) have strong absorption in the UV range (200–420 nm) with a PL spectrum in the 400–600 nm range (Fig. 7a).[118] BN-C-dots exhibit a very bright blue color both in the liquid phase and solid phase upon UV illumination (Fig. 7c). The emission spectrum of BN-C-dots showed excitation-independent behavior (Fig. 7b), which is very different from the excitation-dependent PL in N doped C-dots.[3] Both BN-C-dots and N doped C-dots have a similar size and size distribution; the different PL behavior indicates that the origin of the tunable PL of N doped C-dots is not the quantum confinement effect but the intrinsic surface states.[118] Time-correlated single-photon counting (TCSPC) and fluorescence upconversion spectroscopy measurements for both types of C-dots indicate that either several competing deactivation pathways or a broad distribution of recombination rates exist in excited C-dots (Fig. 7d and e). The shorter weight-averaged lifetime for N-C-dots than for BN-C-dots indicates the higher QY for B and N co-doped C-dots.[118]

UV C-dots only absorb 4% of solar radiation, which is not suitable for fabricating single-layer LSCs. To expand the absorption range of C-dots, large size or graphitization degree C-dots were designed and synthesized.[67] Miao *et al.* reported the synthesis of multiple-color-emission C-dots using CA and urea as precursors through controlling the extent of graphitization and the amount of surface functional groups, –COOH.[67] Fig. 8 shows the results of UV-visible spectra, PL, and PL excitation spectra of the C-dots. The absorption spectrum is ranging from 300 to 600 nm with emission from 400 to 700 nm. The PL excitation spectra of the C-dots indicate that the emission mainly comes from the absorption bands from the n–π* transition of the aromatic sp^2 system containing C=O and C=N bonds.[67] The blue C-dots exhibit an excitation-dependent emission property, while the green and red C-dots have excitation independent emission (Fig. 8a–c).[67] To further absorb more solar light, NIR C-dots have also been synthesized with absorption ranging from 300 to 900 nm, which allows for efficient capture of solar radiation.[116]

3.3 Stokes shift in C-dots

Reabsorption is one of the leading factors for energy loss in large-area LSCs.[30,32] The Stokes shift is defined as the energy gap between the first-excitonic absorption energy band and the maximum PL energy band. A small Stokes shift will lead to strong reabsorption energy loss in large-area LSCs.[30,32,46,119] Even in some fluorophores where the QY could reach 100%, energy could also be lost through number 2. Meanwhile, due to the Stokes shift, the optical efficiency decreases in each cycle of reabsorption. In some of the C-dots reported in the literature, they have a relatively large Stokes shift (200 to 840 meV),[74,96,103,104,118] which is comparable to the large Stokes shift reported for inorganic QDs.[39,40,51,53,120,121] UV C-dots have a large Stokes shift of 275–840 meV (Table 2).[74,103,104,118] Some visible C-dots have a large Stokes shift in the range of

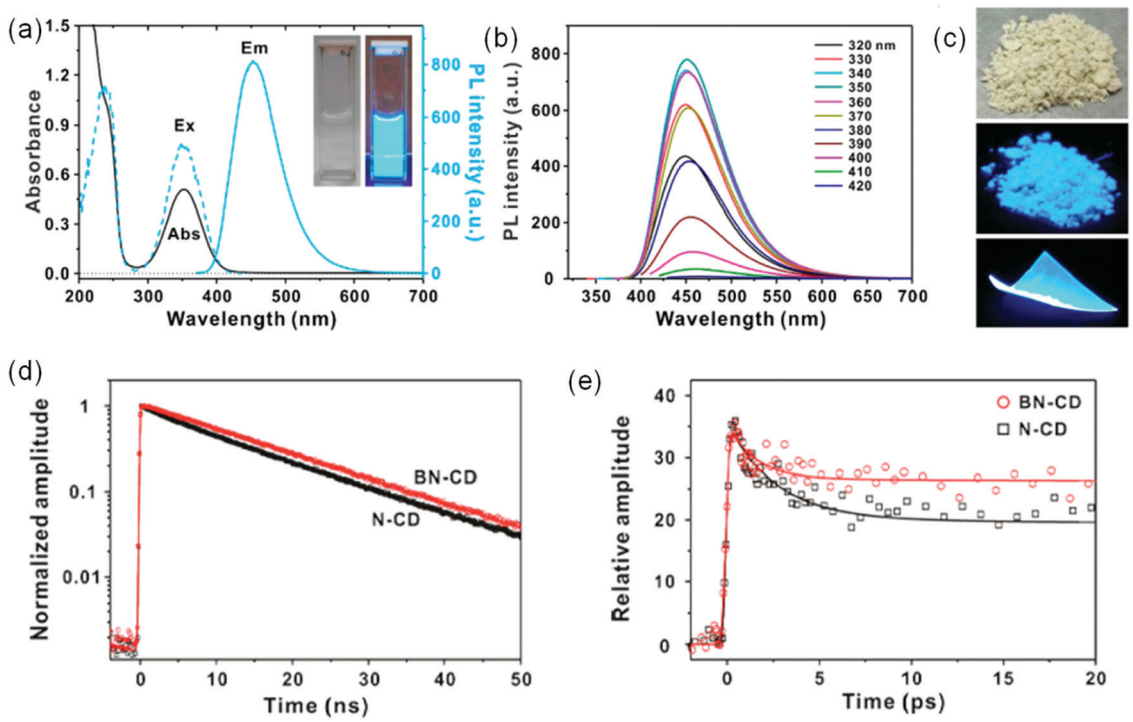

Fig. 7 (a) UV-visible absorbance and PL spectra of BN co-doped C-dots (BN-CD). The inset shows a BN-CD suspension (left) under room light and (right) UV illumination at 365 nm. (b) PL spectra of BN-CD under varying excitation wavelengths from 320 to 420 nm. (c) The bulk production of BN-CD powder and a PVA film under daylight and 365 nm illumination. (d) Normalized PL decay profiles of C-dots obtained by using TCSPC and monitored at 450 nm with excitation at 375 nm. (e) Femtosecond-resolved PL decay kinetics of C-dots measured using PL upconversion and probed at 450 nm with excitation at 365 nm. Reproduced with permission from ref. 118. Copyright 2017, American Chemical Society.

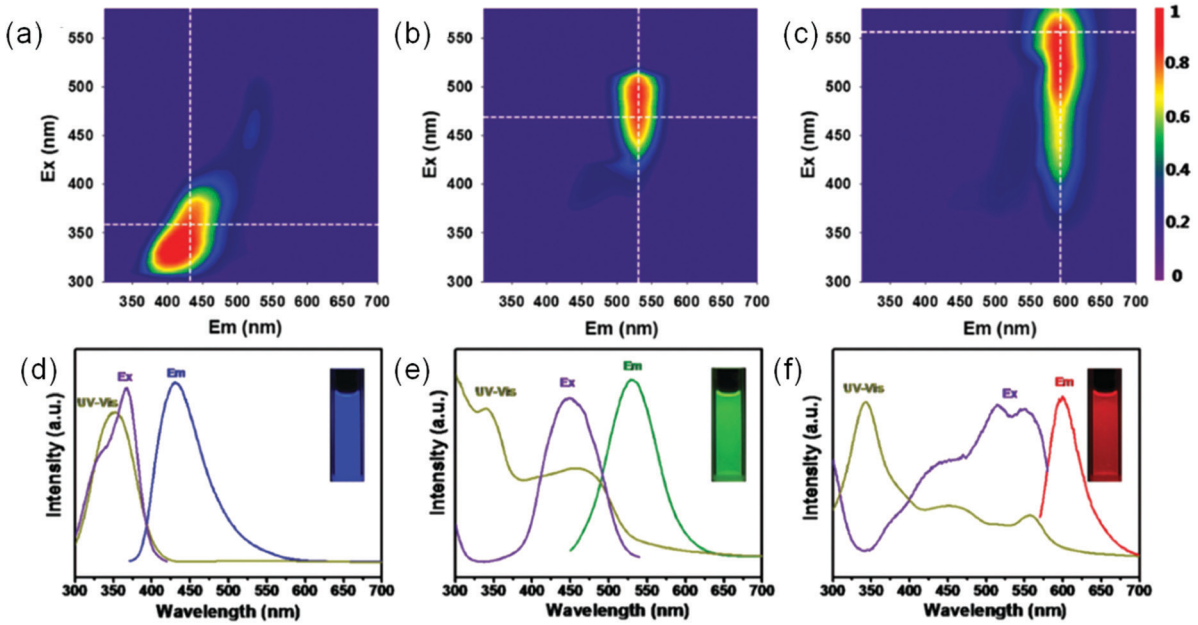

Fig. 8 (a–c) Excitation–emission matrix for blue color C-dots (a), green color C-dots (b), and red color C-dots (c). (d–f) The corresponding absorption, PL, and PL excitation spectra of blue color C-dots (d), green color C-dots (e), and red color C-dots (f). Reproduced with permission from ref. 67. Copyright 2017, American Chemical Society.

Table 2 The optical properties of the C-dots synthesized *via* various types of methods using different precursors

Precursors/solvents	Methods	Absorption range (nm)	QY (%)	Stokes shift (meV)	Ref.
CA, diaminonaphthalene/ethanol	Solvothermal	300–420	70	275	103
CA, ethylenediamine, boric acid/water	Microwave	300–400	80	786	118
CA, THAM/water	Hydrothermal	300–400	99	840	74
CA, cysteamine hydrochloride/water	Hydrothermal	300–400	80	637	104
CA, urea, $CaCl_2$/water	Vacuum heating	300–500	65	530	96
Graphene oxide, polyethylenimine/water	Air-free furnace heating	300–490	99	550	122
CA, urea, OLA/DMF	Solvothermal	300–500	30	453	3
N,*N*-Dimethyl-paraphenylenediamine/DMF	Solvothermal	300–650	86	310	102
CA, 2,3-diaminonaphthalene/ethanol	Solvothermal	300–600	12	426	123
CA, urea/DMF	Solvothermal	300–600	13	128	67
L-Glutamic acid, *o*-phenylenediamine, sulfuric acid/ethanol, water	Solvothermal	300–660	43	220	70
1,4-Diaminonaphthalene/ethanol	Solvothermal	300–600	82	37	128
CA, urea/DMF	Solvothermal	300–900	10	80	116
1,3-Dihydroxynaphthalene, KIO_4/ethanol	Solvothermal	300–600	53	365	129

100–550 meV (Table 2).[86,122,123] Khan *et al.* reported C-dots synthesized *via* an air-free furnace heating method, which have a Stokes shift of 550 meV.[122] Li *et al.* synthesized visible C-dots with absorption/emission in the NIR range, and the as-synthesized C-dots have a Stokes shift of 80 meV.[116] The mechanism of the large Stokes shift in these C-dots is still not very clear. The possible factors affecting the Stokes shift of C-dots could be the defect-state emission mechanism, surface-state emission mechanism and doped-state emission mechanism.[74,96,103,104,118] For instance, Qu *et al.* reported that Na^+ capped C-dots have good separation of the absorption and emission spectra, compared to un-treated C-dots.[86] Usually good surface capping can improve the surface passivation of C-dots, thus decreasing the trap-absorption in the long-wavelength range.[86] As shown in Fig. 9a, the green-color C-dots have a very large Stokes shift (0.53 eV), because of the defect related PL spectrum.[96] There is very small overlap between the absorption and emission spectra. The as-synthesized C-dots have a very narrow size distribution, leading to a uniform energy band gap, with excitation-independent emission. All these properties indicate that the C-dots produced by vacuum-heating are a promising candidate as highly-efficient fluorophores for LSC application. Jia *et al.* reported the red color C-dots with a large Stokes shift of 0.31 eV (Fig. 9b and c).[102] This large Stokes shift could be due to both the narrow size distribution ($\sigma < 14\%$) and efficient surface passivation by NR_2 groups (R = Me, Et and Pr).[102] In addition, the C-dots have a QY as high as 86%, while this type of C-dots was synthesized using very toxic and air-unstable *N*,*N*-dimethyl-, *N*,*N*-diethyl-, and *N*,*N*-dipropyl-paraphenylenediamine precursors, limiting their potential

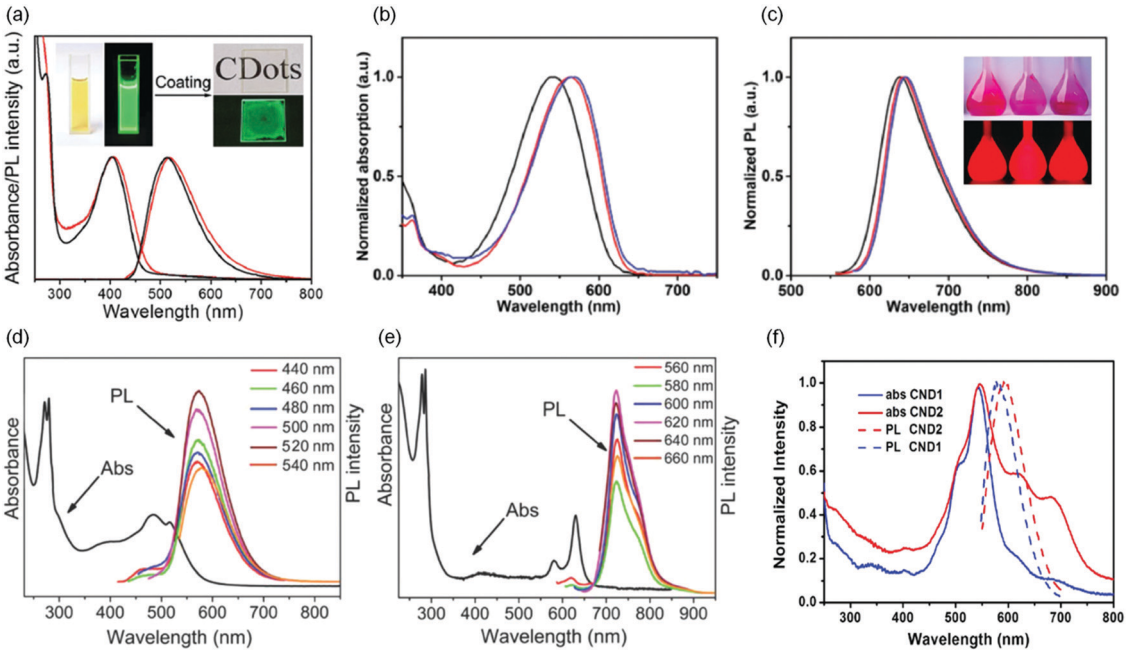

Fig. 9 (a) UV-visible absorption spectra and PL spectra of the purified C-dots synthesized *via* a vacuum heating approach in ethanol solution (black lines) and in a close-packed film (red lines). The insets show the corresponding photographs taken under sunlight and UV light, respectively. (b and c) Normalized UV-visible absorption (b) and PL emission spectra (c) of C-dots prepared through a solvothermal reaction. The inset of (c) is the photograph of the C-dots using different precursors under room light (top) and UV illumination (bottom). (d and e) Absorption and PL spectra of (d) yellow color C-dots and (e) red color C-dots under excitation at different wavelengths. (f) UV-visible absorption and PL spectra (540 nm excitation) of NaOH treated C-dots (CND1) and untreated C-dots (CND2) in dilute ethanol solution. (a) Reproduced with permission from ref. 96. Copyright 2019, Royal Society of Chemistry. (b and c) Reproduced with permission from ref. 102. Copyright 2019, Wiley-VCH. (d and e) Reproduced with permission from ref. 70. Copyright 2018, Wiley-VCH. (f) Reproduced with permission from ref. 86. Copyright 2016, Wiley-VCH.

application in opto-electronic devices.[102] Zhou *et al.* reported the control of the Stokes shift of C-dots through conjugated sp^2-domain controlling and surface charge engineering.[3] With oleylamine (OLA) treatment, the surface of the C-dots can be effectively passivated by OLA, thereby reducing electron transitions from surface states, minimizing the absorption of the C-dots in the range of 550–700 nm, leading to a decrease of the overlap between the absorption and emission spectra. Even though in UV C-dots, the Stokes shift is very large, the Stokes shift in most visible and NIR C-dots is small. In addition, due to the wide size distribution of the as-produced C-dots, the PL spectrum is broader compared to inorganic QDs, leading to a significant overlap between the absorption and PL spectra, which also induces the reabsorption energy loss. It is highly desirable to synthesize visible and NIR C-dots with large Stokes shift (small absorption/emission spectral overlap).

3.4 QY in C-dots

Great efforts have been made to produce C-dots with high QY, which is one of the key parameters for high-efficiency LSCs. As shown in Table 2, we summarized some C-dots which have excellent optical properties for large-area and high-efficiency LSCs. UV C-dots have a typical absorption in the range of 300–400 nm with a very large Stokes shift and high QY of 70–99%.[74,103,104] For example, Zhang *et al.* reported that UV C-dots synthesized using CA and tris(hydroxylmethyl)aminomethane (THAM) as precursors have a QY as high as 99%.[74] These UV C-dots have excitation-independent emission, due to the trap/defect state emission. In addition, these UV C-dots are highly photostable.[74,103] As reported, some UV C-dots have molecular state emission, which is not photostable.[96] For visible C-dots, they have typical absorption in the UV-visible range. The QY of visible C-dots is highly dependent on their synthetic method, emission nature and surface functional groups.[102,122,123] The C-dots synthesized using graphene oxide represent the highest QY so far for visible C-dots, reaching 99%.[122] However, in NIR C-dots, even though the C-dots have a wide spectrum covering from the UV to the visible and NIR range, the QY is still very low (less than 20%).[116] Further improvement of the QY in NIR C-dots could be achieved focusing on the selection of synthetic approaches, deep investigation of the PL nature and surface-post treatment. For example, one could produce C-dots with a uniform energy band gap by synthesizing C-dots with a very narrow size distribution (*e.g.* the vacuum heating approach), which could largely avoid aggregation-induced emission, considering that the C-dots should be embedded in a solid film. The C-dots in a solid film could have a similar QY to that in solution.[96]

With respect to inorganic QDs, dyes/polymers and perovskite NCs, most C-dots have excellent stability regarding the thermal-, chemical-, colloidal- and photostability.[27,51,119,124–126] During the synthesis, purification, and application, it is not necessary to handle the C-dots in air-free conditions, and this presents a promising potential for applications in opto-electronic devices.[59,61,89,93,99,102,123,126,127]

4. LSCs based on C-dots

C-dots have been widely used as efficient fluorophores for LSC fabrication.[8,9,16,43,106,107,119,126,127,130–137] Table 3 summarizes the most recent research on LSCs based on various types of C-dots compared with other fluorophore based LSCs (*e.g.* core/shell QDs, perovskite QDs, dyes and Si QDs). In this section, we also introduce recent advances in the optimization of the configuration of LSCs in order to improve the optical efficiency and long-term stability of LSCs.[3,106,130]

4.1 Single-layer LSCs based on C-dots

Zhou *et al.* developed an LSC using OLA modified C-dots as fluorophores.[3] The visible C-dots were synthesized by a solvothermal method with a QY of 30%. After surface treatment with OLA, the C-dots can be transferred into nonpolar solvents because of the long hydrophobic carbon chain. As shown in Fig. 10a, in the presence of a catalyst and bifunctional group, the OLA can link to the surface of the C-dots. Fig. 10b shows the absorption and PL spectra of the C-dots before and after different surface treatments. The absorption in the long-wavelength range (550–700 nm) reduced and the overlap between the absorption and emission spectra decreased after surface treatment. The PL decay in Fig. 10c reveals the decrease of the lifetime after surface treatment, consistent with the increase of the QY.[86] The poly(lauryl methacrylate) (PLMA) polymer was selected as the host material for LSCs because of its excellent properties for LSC fabrication (*e.g.* high transparency, high refractive index and good stability). The OLA-modified C-dots were applied to fabricate LSCs ($10 \times 1.5 \times 0.2$ cm^3) by embedding them into the PLMA polymer matrix (Fig. 10d). Under sunlight illumination, the concentrated yellow light emitted from the edges of the LSCs is clearly visible. The emission spectra of OLA-modified C-dots embedded in LSCs as a function of the optical path are shown in Fig. 10e. The PL spectra exhibit a red-shift with the increase of the optical path. The PL peak position and shape were almost unchanged, suggesting the suppression of reabsorption loss in the LSCs. The maximum η_{opt} of the LSCs based on C-dot/PLMA polymer reached 1.2% with dimensions of $2 \times 1.5 \times 0.2$ cm^3 (with a mirror placed on the bottom of the LSC). The surface treatment can significantly improve the surface passivation of the C-dots, thus enhancing both the Stokes shift and the QY. Due to the lower QY compared to inorganic QDs, the obtained η_{opt} is still far below that of LSCs based on inorganic QDs.

Talite *et al.* fabricated film structured LSCs by *in situ* cross-linking organosilane-functionalized carbon nanodots (Si-CNDs) to form a solid-state thin film on a glass substrate.[105] Such LSCs based on cross-linked Si-CNDs can hold high optical performance and film uniformity even under high-loading conditions (Fig. 10f). With the increase of the loading content, the absorbance of the LSCs increases and no tails extend to the longer wavelength range, further confirming high optical quality and film uniformity (Fig. 10g). Thanks to the high optical quality and film uniformity, which reduce the scattering losses, such LSCs ($3 \times 3 \times 0.3$ cm^3) with 25 wt% loading still hold a high edge-emission efficiency of 68% (Fig. 10h), and yield an internal quantum efficiency (the ratio between the energy of emitted photons and absorbed photons) of 22% and external quantum efficiency (the ratio between the energy of emitted photons and incident photons) of 12% at a wavelength of 354 nm. They further developed Si-CNDs with an ultrahigh QY of 94% by surface/interface engineering C-dots crosslinked in a siloxane matrix, and fabricated film structured visible-transparent LSCs based on the Si-CND@siloxane composite deposited on a glass substrate. The LSC has a high internal quantum efficiency of 66% and external quantum efficiency of 3.9%.[134]

Gong *et al.* used N-doped C-dots as fluorophores to fabricate film structured LSCs.[9,106,130] As shown in Fig. 11a and b, the reported N-doped C-dots exhibit a broad absorption spectrum

Table 3 η_{opt} of LSCs based on different types of QDs

Type of LSC	Fluorophores	Dimensions (cm^3)	η_{opt} (%)	Ref.
Core/shell QD slab	PbS/CdS	$10 \times 1.5 \times 0.2$	1.0	46
Core/shell QD slab	CdSe/CdS	$21.5 \times 1.35 \times 0.5$	0.6	138
Core/shell QD film[a]	CdSe/CdS	$10 \times 10 \times 0.4$	2.95	139
Core/shell QD slab[a]	CdSe/CdS	$8 \times 8 \times 0.7$	3.44	140
Core/shell QD slab	$CuInSe_xS_{2-x}$/ZnS	$12 \times 12 \times 0.3$	3.2	41
Core/alloyed-shell QD slab	$CdSe/Cd_xPb_{1-x}S$/CdS	$7 \times 1.5 \times 0.3$	1.4	141
Core/alloyed-shell QD film	SiO_2-coated $CdSe/Cd_{1-x}Zn_xS$	$10.2 \times 10.2 \times 0.16$	1.9	121
Perovskite QD film	Cs_4PbBr_6	$10 \times 10 \times 0.4$	2.4	51
Perovskite QD slab	$CsPb(Br_{0.2}I_{0.8})_3$	$9 \times 1.3 \times 0.2$	2.0	45
Dye film[b]	DCJTB; Pt (TPBP)	$2.5 \times 2.5 \times 0.4$	6.8	142
Dye slab[b]	Lumogen F Red305; fluorescence yellow; CRS040	$5 \times 5 \times 1$	7.1	143
Si QD/PLMA slab	Si	$12 \times 12 \times 0.26$	2.85	40
C-dots[b]	Blue C-dots; yellow C-dots	$10 \times 10 \times 0.8$	1.1	3
C-dots[a]	C-dots	$10 \times 10 \times 0.9$	1.6	126
C-dot/PMMA film	N-doped C-dots	$2.5 \times 1.6 \times 0.1$	4.75	106
C-dot/PVP film	N-doped C-dots	$2 \times 2 \times 0.2$	4.97	130
C-dot/PMMA slab	N-doped C-dots	$2 \times 2 \times 0.2$	12.23	9
C-dots and core/shell QDs[b]	C-dots; CdSe/CdS	$10 \times 10 \times 0.4$	1.4	8
C-dots and perovskite QDs[b]	C-dots; $CsPb(Br_xI_{1-x})_3$; $CsPb(Cl_xBr_{1-x})_3$	$10 \times 10 \times 0.6$	3.05	131
C-dots[b]	Blue C-dots; green C-dots; red C-dots	$10 \times 10 \times 0.8$	2.3	144

[a] The LSC has a laminated structure. [b] The LSC has a tandem structure.

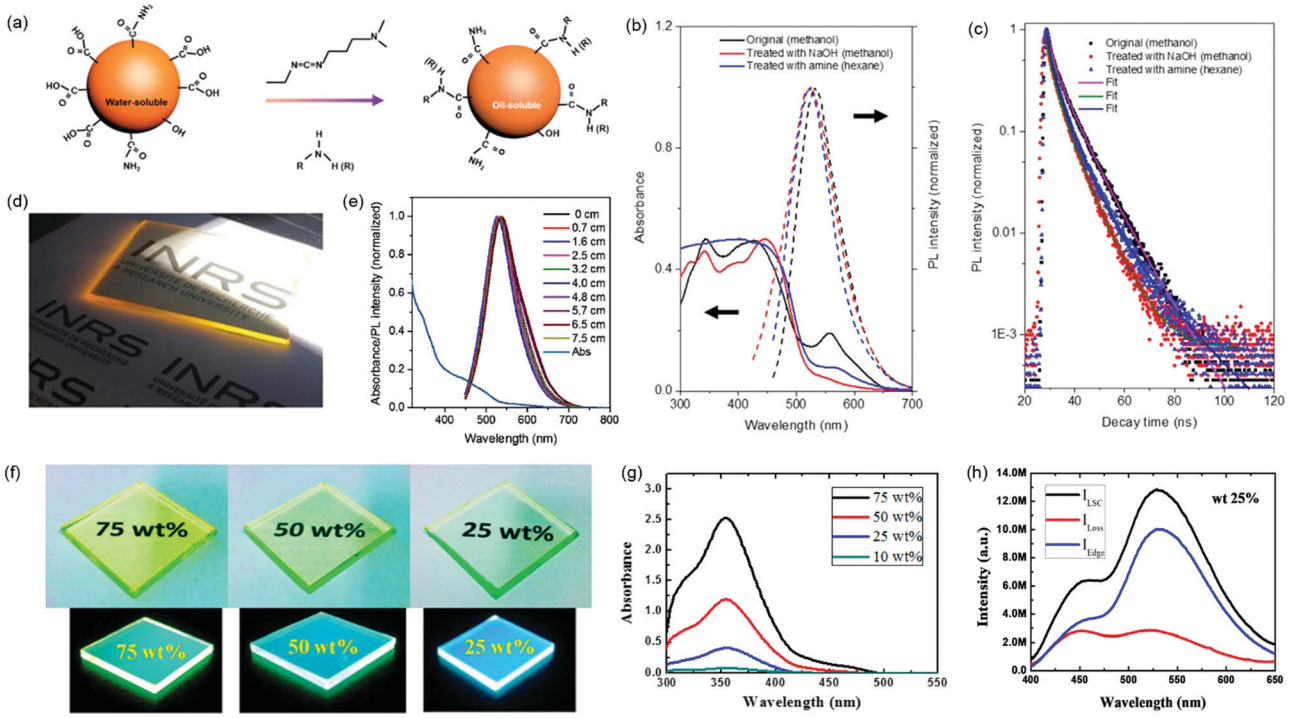

Fig. 10 (a) Schematic illustration of surface modification of C-dots before and after phase transfer. Absorption and PL spectra (b) and PL decay curves collected at an emission peak of 540 nm (c) of C-dots under different surface treatments (excitation wavelength at 440 nm). (d) Photograph of colorless large-area OLA modified C-dots based LSCs with dimensions of $10 \times 10 \times 0.2$ cm^3 under one sun illumination. (e) Absorption and PL spectra measured at different optical paths for the OLA-modified C-dots based LSCs. (f) Photographs of cross-linked Si-CNDs with different loading contents under ambient-light and UV-light illumination. (g) Absorption spectra of the cross-linked Si-CNDs with different loading contents. (h) PL emission spectra of cross-linked Si-CNDs with 25 wt% loading collected from all surfaces, facial surfaces, and edge surfaces. (a–e) Reproduced with permission from ref. 3. Copyright 2018 Elsevier. (f–h) Reproduced with permission from ref. 105. Copyright 2018, American Chemical Society.

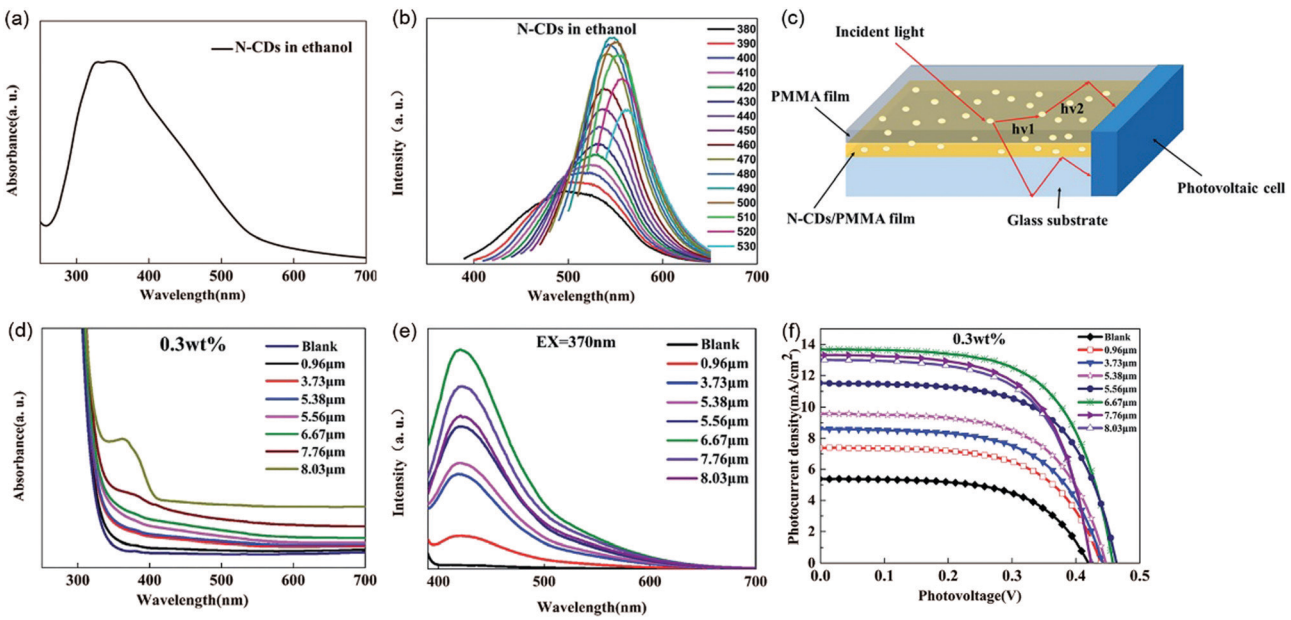

Fig. 11 (a) UV-vis spectrum of N-doped C-dots in ethanol. (b) PL spectra of N-doped C-dots dispersed in ethanol excited by light with different wavelengths. (c) Schematic illustration of the N-doped C-dot/PMMA film LSC. Absorption (d) and PL spectra (e) of N-doped C-dot/PMMA thin film LSCs with different thicknesses (0.3 wt% N-doped C-dots). (f) Relationship of the photocurrent density and photovoltage (J–V) of the N-doped C-dot/PMMA thin films with different film thicknesses (0.3 wt% N-CDs). Reproduced with permission from ref. 106. Copyright 2017 The Royal Society of Chemistry.

from 300 nm to 600 nm and an excitation dependent PL shifting from 500 nm to 562 nm. Upon spin coating an N-doped C-dot/polymethyl methacrylate (PMMA) mixture on top of glass slides, the LSCs with different film thicknesses were prepared (Fig. 10c). The optical properties of the N-doped C-dot/PMMA film LSCs with various thicknesses were investigated and are shown in Fig. 11d–f. Due to the fact that more N-doped C-dots are contained in the thicker film, the absorption intensity of the LSCs increases with the film thickness increases. The PL spectra of the N-doped C-dot/PMMA film LSCs display an intensity increase first and then gradually decrease with the increase of the film thickness (Fig. 11e). When one side of the LSCs is covered by PV cells, the photocurrent density was similar to the intensity change of PL spectra with the film thickness increases (increases first until the film thickness reached 6.67 μm and then slightly decreases) (Fig. 11f). And they achieved an optimal optical efficiency of 4.75% when the N-doped C-dot/PMMA film thickness is 6.67 μm.[106] They further used the N-doped C-dots as phosphors to be embedded into a polyvinylpyrrolidone (PVP) thin film for LSC fabrication and achieved a η_{opt} of 5.02% and a PCE of 4.97%.[130] They further studied the effect of the C-dot concentration effect on the optical efficiency of the LSCs.[9] When the concentration of N-doped C-dots in the LSC slabs is 0.08 wt%, the optimal optical efficiency is 12.23%. The successful fabrication of such doped C-dots based LSCs provides a guideline for eco-friendly LSC based energy-building integration. However, the best optical efficiency of C-dots based LSCs is still rather low. Up to now, in single-layer LSCs, the C-dots can only absorb sunlight in the UV and visible range. It is highly desired to synthesize C-dots with absorption covering from the UV-visible to the NIR range, in order to enhance the optical efficiency of LSCs.

In addition, polymers are used as key components in LSCs, which affects the performance of the LSCs. Typically, the polymers should be optically transparent from the UV-visible to the NIR region and compatible with the fluorescent materials, have good stability and be easy to process into waveguides or films. The refractive index is an important factor that affects the optical efficiency of LSCs. The refractive index of the polymers mainly determines the surface reflection (Fig. 1, number 1) and trapping efficiency (Fig. 1, number 2) of the LSCs. This means that the polymers used as waveguides in LSCs should possess a refractive index optimized for a balance between the surface reflection and trapping efficiency, which requires $(1 - R)\eta_{TIR}$ to be maximized. PMMA, PLMA and PVP are three popular polymers as host materials in C-dots based LSCs. The refractive index of PVP (1.53) is higher than that of PMMA (1.49) or PLMA (1.47).[145] Thus, PVP exhibits higher trapping efficiency than PMMA and PLMA with the same shape and transparency.

4.2 Laminated LSCs based on C-dots

Except for the optimization of the fluorophore properties, the adjustment of the device structure is another efficient way to enhance the optical efficiency of LSCs.[25] Compared to single-layer LSCs, laminated LSCs can improve the optical efficiency of the devices by decreasing the energy loss due to the decrease of the geometric factor (G, defined as the ratio of the top area and the edge area).[38,139,140,146] Zhao *et al.* reported laminated LSCs using C-dots as fluorophores.[126] The C-dots used in laminated LSCs have an absorption spectrum ranging from 300 nm to 550 nm and a PL spectrum ranging from 400 nm to 700 nm (Fig. 12a). The laminated LSCs were prepared by drop-casting a C-dot/PVP methanol solution on a glass substrate. After drying, another glass slide was placed on the top of the C-dots/PVP film (Fig. 12b and c). By optimizing the C-dot concentration in PVP, the laminated LSCs achieved a η_{opt} of 1.6%. Compared to single-layer LSCs, the laminated LSCs based on C-dots have much higher optical efficiency because of their smaller G factor (with identical dimensions). In addition, the C-dots can be encapsulated inside the glass and avoid direct contact with oxygen, water or chemicals, which can significantly improve the long-term stability of the devices. However, in these structured LSCs, the amount of silicon solar cells is much more compared to single-layer LSCs, which increases the cost of electricity.

4.3 Tandem structured LSCs based on C-dots

Compared to single-layer LSCs or laminated LSCs, Zhou *et al.* first reported tandem structured LSCs based on two types of C-dots (Fig. 13c).[3] The UV C-dots in the top layer have an absorption spectrum range of 300–400 nm with a large Stokes

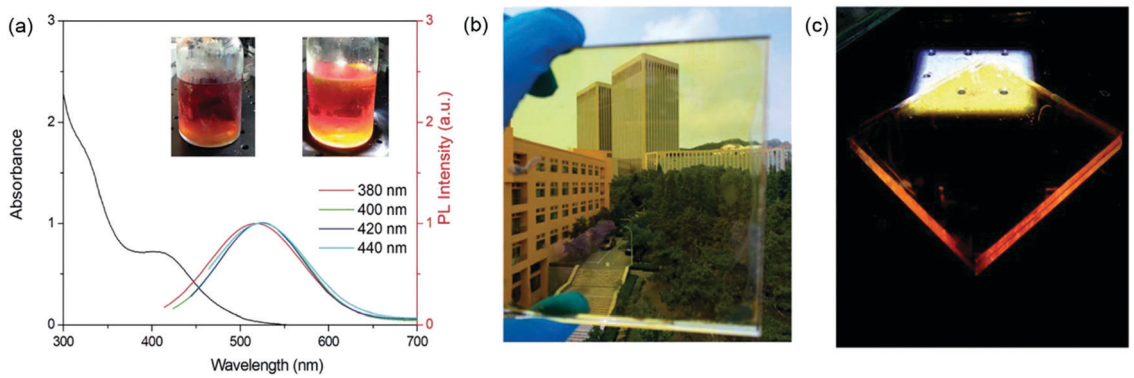

Fig. 12 (a) Absorption and PL spectra of C-dots dispersed in methanol solution. The excitation wavelength is 380–440 nm. Photographs of the LSC under ambient (b) and one sun (100 mW cm^{-2}) illumination (c). Reproduced with permission from ref. 126. Copyright 2019 Elsevier.

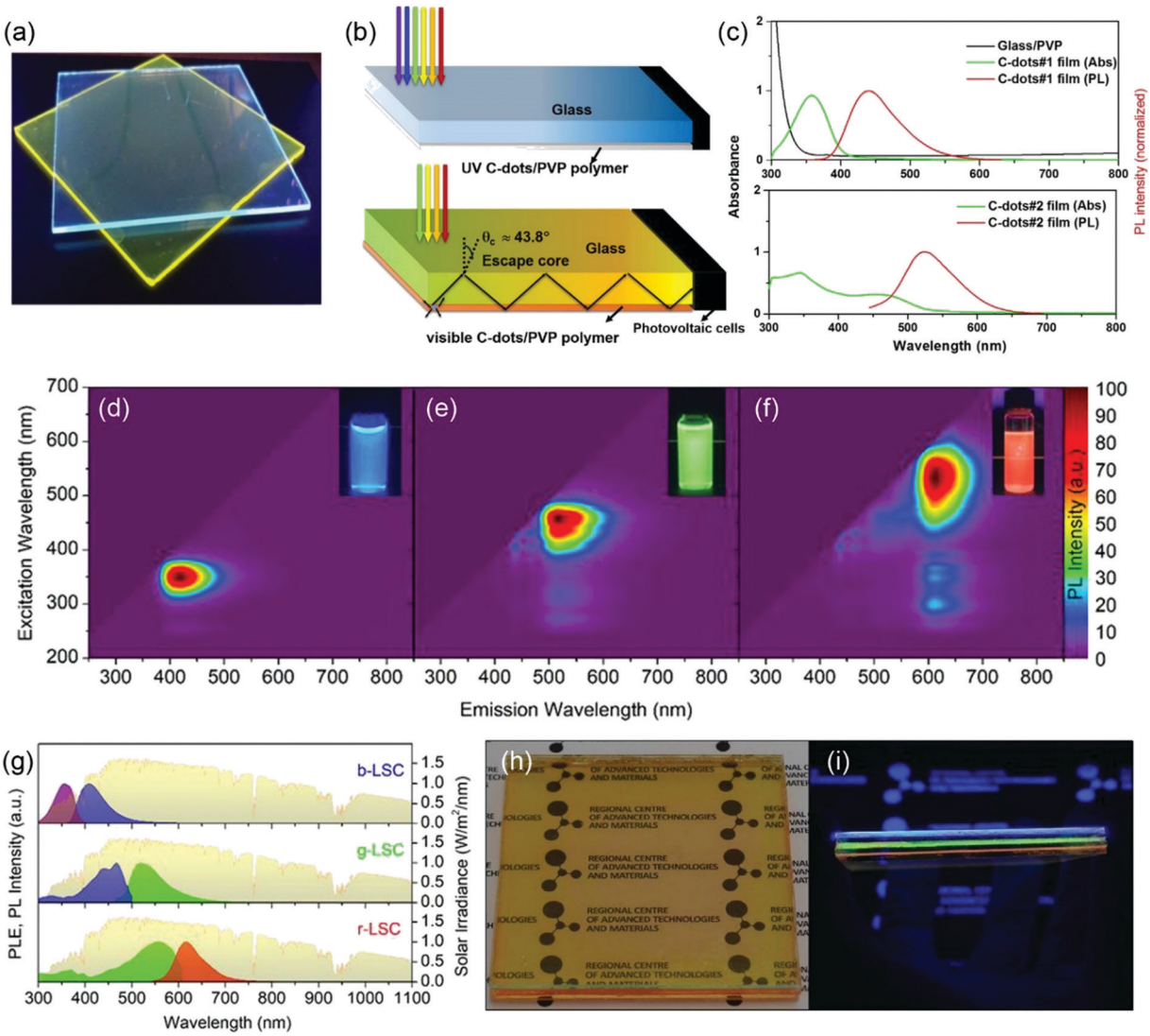

Fig. 13 Photograph (a) and schemes (b) of tandem thin-film LSCs based on UV C-dots (top) and visible C-dots (bottom). (c) The absorption and emission spectra of UV C-dots (#1, top) and visible NaOH treated C-dots (#2, bottom) based thin-film LSCs and absorption spectrum of PVP on a glass substrate. (d–f) Excitation–emission color maps of blue, green and red C-dots. Insets: Photographs of the corresponding C-dots solution under UV light. (g) PL excitation and emission spectra of individual LSCs based on blue, green and red C-dots compared with the AM 1.5 solar spectrum (in yellow). Photograph of the tandem LSC under daylight (h) and weak UV illumination (i). (a–c) Reproduced with permission from ref. 3. Copyright 2018 Elsevier. (d–i) Reproduced with permission from ref. 144. Copyright 2020 The Royal Society of Chemistry.

shift and a high QY of 60% (Fig. 13c, top panel). The visible C-dots in the bottom layer have a broad absorption ranging from 300 nm to 550 nm, with a QY of 40% (Fig. 13c, bottom panel). The as-prepared tandem LSC has a η_{opt} of 1.1% with a dimension of 10 × 10 × 0.2 cm^3. However, the as-fabricated tandem LSC can only absorb sunlight in the wavelength range of 300–550 nm. To further extend the absorption range of the Sun's spectrum, Zdražil *et al.* fabricated a tandem LSC with three layers using three types of C-dots.[144] As shown in Fig. 12d–f, highly luminescent blue, green and red emissive C-dots were synthesized. By drop-casting the C-dot/polymer solution onto glass substrates, individual C-dots based LSCs were fabricated. The PL excitation and emission spectra of the three individual LSCs are shown in Fig. 13d–f. The excitation spectra of the three LSCs extend over the entire visible light wavelength range, which allows efficient capture of solar radiation (Fig. 13g). By composing together all the three individual C-dots based LSCs, a tandem LSC was fabricated, as shown in Fig. 13h and i. The tandem LSC appears transparent in ambient light with an orange color (Fig. 13h). Blue, green and red light are visible from the edge of the LSC under UV illumination (Fig. 13i). The fabricated tandem LSC (8 × 8 cm^2) based on blue, green and red C-dots exhibits an internal quantum efficiency of 23.6% and η_{opt} of 2.3%. Under 1 mW cm^{-2} continuous monochromatic illumination, the PL intensity of the three individual C-dots based LSCs showed no significant drop over 10 hours, indicating excellent photostability of the C-dots based LSCs.

Because C-dots have excellent photostability compared to inorganic QDs or perovskite NCs, Zhao *et al.* have used C-dots to improve the photostability of LSCs based on perovskite QDs by absorbing sunlight in the UV range.[131] As shown in Fig. 14a, the fluorophore in the top layer is the C-dots and the fluorophores in the second and third layers are $CsPb(Br_{1-x}Cl_x)_3$ and $CsPb(Br_xI_{1-x})_3$ perovskite QDs, respectively. The C-dots film layer can absorb sunlight ranging from 300 to 400 nm and the perovskite layers can absorb sunlight ranging from 400 to 650 nm (Fig. 14b). The as-fabricated tandem LSC based on C-dots and perovskite QDs exhibits a η_{opt} of 3.05% under one sun illumination (100 mW cm^{-2}), which improves 117% and 27% compared to the single-layer LSCs based on $CsPb(Br_{1-x}Cl_x)_3$ and $CsPb(Br_xI_{1-x})_3$ QDs, respectively. Similarly, tandem LSCs comprising two layers (a C-dots layer and a CdSe/CdS QDs layer) were fabricated to improve the optical efficiency of the single-layer LSCs (Fig. 14c).[8] The η_{opt} of this tandem LSC is 1.4%, which represents a 16% improvement in efficiency over single-layer LSCs based on CdSe/CdS QDs. In addition to the enhancement of the efficiency for LSCs, the tandem LSCs with a C-dots top layer can enhance the photostability of the LSCs based on perovskite QDs or CdSe/CdS QDs due to the excellent photostability of C-dots and their strong absorption of UV light. As shown in Fig. 14d, upon 70 h UV illumination, the CdSe/CdS QDs based LSC with the C-dots thin film as a top protective layer retains 75% of its initial integrated PL intensity, which is 1.8 times that of the LSC without the C-dots layer. Besides improving the η_{opt} of LSCs based on inorganic QDs or perovskite NCs, C-dots have been used as the top layer in tandem LSCs aiming to improve the η_{opt} of LSCs based on organic dyes.[127,147] In the above tandem LSCs consisting of C-dots and inorganic or organic emissive luminescent materials, the use of C-dots can enhance both the optical efficiency and photostability of the LSCs, while the amount of silicon solar cells increases with the increasing number of LSC layers. In addition, the fluorophores in tandem structured LSCs are still exposed to the surrounding environment, similar to single-layer LSCs. Compared to single-layer or tandem LSCs, laminated LSCs can give much better long-term stability, which presents the most advantages for further potential applications.

5. Potential applications

LSCs can convert sunlight into concentrated fluorescence on the edges of the devices. By coupling with different optoelectronic

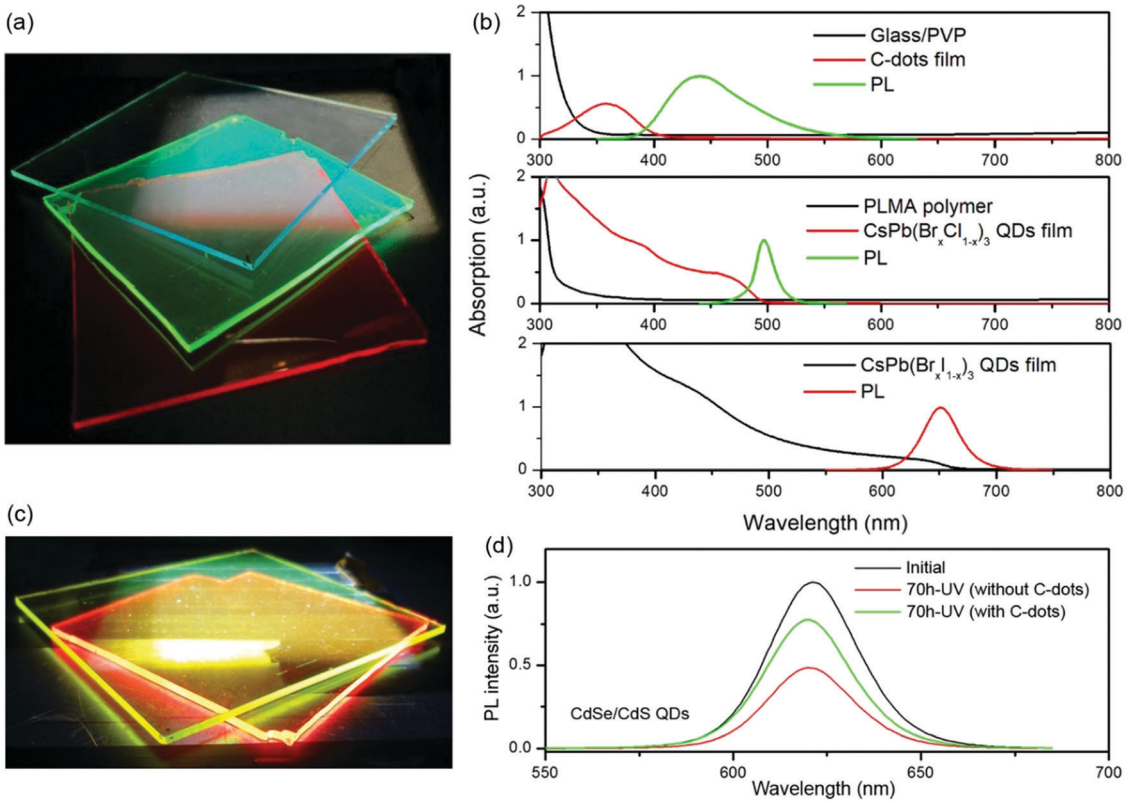

Fig. 14 (a) Photograph of the tandem LSC based on C-dots, and $CsPb(Cl_{0.2}Br_{0.8})_3$ and $CsPb(Br_{0.2}I_{0.8})_3$ perovskite QDs under one sun illumination. (b) Absorption and normalized PL spectra of LSCs based on C-dot/PVP on a glass substrate, and $CsPb(Br_{0.8}Cl_{0.2})_3$ QDs and $CsPb(Br_{0.2}I_{0.8})_3$ QDs incorporated into a PLMA polymer matrix. The excitation wavelength is λ_{ex} = 350 nm for the C-dots and λ_{ex} = 444 nm for the perovskite QDs. (c) Photograph of the tandem LSCs comprising C-dots and CdSe/CdS QDs under one sun illumination. (d) PL spectra of the LSCs based on CdSe/CdS QDs before and after 70 h UV illumination under ambient conditions with or without a protective layer based on C-dot/PVP. (a and b) Reproduced with permission from ref. 131. Copyright 2018 Elsevier. (c and d) Reproduced with permission from ref. 8. Copyright 2018 The Royal Society of Chemistry.

devices, the fluorescence can be converted to electricity or fuels (*e.g.* hydrogen). For example, LSCs have been coupled with PV cells for BIPV systems due to their light weight, adjustable transparency, low-cost and tunable colors.[28,53,148] LSC–PV systems could be embedded in triple-insulated glass to form PV windows (Fig. 15a).[28] They can also be used as an "Electric Mondrian",[149] in which colorful square and rectangular LSC plates were used to create a decorative element, and PV cells were used at the sides of the LSCs to generate electricity (Fig. 15b). With the appropriate choice of fluorophores in LSCs, LSC–PV systems can be used in greenhouses[150] or solar noise barriers[151] (Fig. 15c and d). As plants mainly absorb sunlight in the wavelength range of 400–520 nm and 610–720 nm, the LSCs should absorb sunlight in other wavelength ranges unused by plants. As a result, the LSC–PV system can generate electricity with a neutral or positive benefit to the underlying plants in the greenhouse. Besides the application in LSC–PV systems, LSCs can be used as light sources for photochemical reactions.[152,153] Liu *et al.* reported the use of LSCs coupled with photoelectrochemical (PEC) hydrogen generation.[153] As shown in Fig. 15e, the emitted red light from LSCs can be collected by the photoanode placed at the edges of the LSCs, and the concentrated light can be used as a light source for PEC hydrogen production. Meanwhile, the fluorophores in the LSC can convert UV light to visible light, improving the stability of the PEC system. To date, there is still no report on using C-dots based LSCs for photo-electrical/chemical applications. Owing to the excellent properties of LSCs based on C-dots, future research should be focused on

Fig. 15 (a) Schematic of a PV window consisting of a semi-transparent, colorless LSC. (b) Photograph of the Electric Mondrian prototype. (c) Photograph of the LSC greenhouse. (d) Photograph of the noise barrier prototype. (e) Schematic diagram of the CdSe/CdSSe/CdS QD sensitized photoanode coupled with an LSC based on CdSe/CdS QDs. (a) Reproduced with permission from ref. 28. Copyright 2015 Elsevier. (b) Reproduced with permission from ref. 149. Copyright 2017 Wiley-VCH. (c) Reproduced with permission from ref. 150. Copyright 2016 AIP publishing. (d) Reproduced with permission from ref. 151. Copyright 2017 Elsevier. (e) Reproduced with permission from ref. 153. Copyright 2019 The Royal Society of Chemistry.

using C-dots as fluorophores for solar-to-electricity or solar-to-fuel applications.

6. Conclusions and perspectives

In summary, we reviewed the most recent advances in LSCs based on colloidal C-dots, highlighting the correlation between the structure and optical properties of C-dots for applications in LSC technologies. We summarized various synthetic strategies developed for the synthesis of high-quality C-dots with respect to a narrow size distribution and highly crystalline structure using green precursors and solvents, including solvothermal, vacuum heating and microwave synthesis *etc.* We further summarized the required optical properties for high-efficiency large-area LSCs, including a wide absorption spectrum, large Stokes shift and high QY, through synthetic method selection, size selection and surface treatment. A detailed account of the latest examples of applications of C-dots for LSCs was summarized, including utilization of various types of C-dots and different configurations of LSCs (*e.g.* single-layer LSCs, laminated LSCs, and tandem structured LSCs). At the end, we gave several potential applications of LSCs in solar-to-electricity and solar-to-fuel conversion. Despite the great effort invested in recent years, a number of challenges still remain unanswered in order to fabricate high-efficiency LSCs based on C-dots. (i) It is still challenging to synthesize C-dots with a narrow size distribution in a large quantity using sustainable precursors and green solvents. (ii) Although some C-dots have a relatively large Stokes shift, there is still a significant overlap between the absorption and emission spectra due to both the absorption tail at long wavelengths and wider emission spectrum compared to inorganic QDs or perovskite NCs. The overlap between the absorption and emission spectra leads to a significant energy loss because of reabsorption in large-area LSCs. This explains why the current obtained η_{opt} in LSCs based on C-dots is still lower than that of LSCs based on inorganic QDs. (iii) The C-dots used for LSCs have limited absorption in the range of 300–600 nm, matching only 40% of the Sun's spectrum. The reported NIR C-dots have a wide absorption spectrum, but they usually have a low QY ($<20\%$), which is not suitable for LSCs at the current stage. Future research directions should be focused on: (1) developing a general synthetic approach which could meet the requirements of reproducible simple synthesis with large scale and excellent optical properties for C-dots. Particularly, the precursors should be easily prepared from earth-abundant elements, using sustainable materials (*e.g.* CA and urea). (2) Synthesizing C-dots with small overlap between the absorption and emission spectra through structure design and PL mechanism study. (3) Synthesis of NIR C-dots with broad absorption up to the NIR range and high QY (close to 100%), by improving the surface functional groups or core/shell structure design. For example, an amorphous silica shell can passivate the surface molecule-like energy state, alleviating the absorption or emission due to the molecular-energy state. (4) Improving η_{opt} of LSCs based on C-dots by selection of high-quality C-dots and optimization of the LSC configuration. Compared to single and tandem structured LSCs, laminated LSCs would have superior advantages, such as high photostability, high optical efficiency and long-lifetime.

Conflicts of interest

The authors declare no conflict of interest.

Acknowledgements

H. Zhao acknowledges the start funding support from Qingdao University and the funding from the Natural Science Foundation of Shandong Province (ZR2018MB001).

Notes and references

1 L. Liu, Q. Xi, G. Gao, W. Yang, H. Zhou, Y. Zhao, C. Wu, L. Wang and J. Xu, *Sol. Energy Mater. Sol. Cells*, 2016, **157**, 937–942.
2 H. Zhao and F. Rosei, *Chem*, 2017, **3**, 229–258.
3 Y. Zhou, D. Benetti, X. Tong, L. Jin, Z. M. Wang, D. Ma, H. Zhao and F. Rosei, *Nano Energy*, 2018, **44**, 378–387.
4 S. H. Lee, M. F. Bhopal, D. W. Lee and S. H. Lee, *Mater. Sci. Semicond. Process.*, 2018, **79**, 66–73.
5 M. Yamaguchi, K. H. Lee, K. Araki and N. Kojima, *J. Phys. D: Appl. Phys.*, 2018, **51**, 133002.
6 F. Navarro-Pardo, H. Zhao, Z. M. Wang and F. Rosei, *Acc. Chem. Res.*, 2018, **51**, 609–618.
7 K. Basu, H. Zhang, H. Zhao, S. Bhattacharya, F. Navarro-Pardo, P. K. Datta, L. Jin, S. Sun, F. Vetrone and F. Rosei, *Nanoscale*, 2018, **10**, 15273–15284.
8 G. Liu, H. Zhao, F. Diao, Z. Ling and Y. Wang, *J. Mater. Chem. C*, 2018, **6**, 10059–10066.
9 X. Gong, W. Ma, Y. Li, L. Zhong, W. Li and X. Zhao, *Org. Electron.*, 2018, **63**, 237–243.
10 J. Liu, G. S. Selopal, H. Zhang, S. Sun, H. Zhao and F. Rosei,, *ACS Photonics*, 2019, **6**, 2479–2486.
11 G. Liu, Z. Ling, Y. Wang and H. Zhao, *Int. J. Hydrogen Energy*, 2018, **43**, 22064–22074.
12 X. Tong, X.-T. Kong, Y. Zhou, F. Navarro-Pardo, G. S. Selopal, S. Sun, A. O. Govorov, H. Zhao, Z. M. Wang and F. Rosei, *Adv. Energy Mater.*, 2018, **8**, 1701432.
13 H. Zhao, G. Liu, F. Vidal, Y. Wang and A. Vomiero, *Nano Energy*, 2018, **53**, 116–124.
14 H. Zhao, J. Liu, F. Vidal, A. Vomiero and F. Rosei, *Nanoscale*, 2018, **10**, 17189–17197.
15 K. Wang, X. Tong, Y. Zhou, H. Zhang, F. Navarro-Pardo, G. S. Selopal, G. Liu, J. Tang, Y. Wang, S. Sun, D. Ma, Z. M. Wang, F. Vidal, H. Zhao, X. Sun and F. Rosei, *J. Mater. Chem. A*, 2019, **7**, 14079–14088.
16 Z. Li, X. Zhao, C. Huang and X. Gong, *J. Mater. Chem. C*, 2019, **7**, 12373–12387.
17 H. Zhao, H. Zhang, G. Liu, X. Tong, J. Liu, G. S. Selopal, Y. Wang, Z. M. Wang, S. Sun and F. Rosei, *Appl. Catal., B*, 2019, **250**, 234–241.

18 I. Alkian, A. Prasetio, L. Anǵǵara, Karnaji, M. H. Fonisyah, Z. M. Rizka and H. Widiyandari, *J. Phys.: Conf. Ser.*, 2019, **1204**, 012093.
19 K. Basu, D. Benetti, H. Zhao, L. Jin, F. Vetrone, A. Vomiero and F. Rosei, *Sci. Rep.*, 2016, **6**, 23312.
20 D. Benetti, K. T. Dembele, J. Benavides, H. Zhao, S. Cloutier, I. Concina, A. Vomiero and F. Rosei, *J. Mater. Chem. C*, 2016, **4**, 3555–3562.
21 H. Bian, Q. Wang, S. W. Yang, C. J. Yan, H. R. Wang, L. Liang, Z. W. Jin, G. Wang and S. Z. Liu, *J. Mater. Chem. A*, 2019, **7**, 5740–5747.
22 M. A. Franzman, C. W. Schlenker, M. E. Thompson and R. L. Brutchey, *J. Am. Chem. Soc.*, 2010, **132**, 4060–4061.
23 G. S. Selopal, H. Zhao, X. Tong, D. Benetti, F. Navarro-Pardo, Y. Zhou, D. Barba, F. Vidal, Z. M. Wang and F. Rosei, *Adv. Funct. Mater.*, 2017, **27**, 1701468.
24 G. S. Selopal, H. G. Zhao, Z. M. M. Wang and F. Rosei, *Adv. Funct. Mater.*, 2020, **30**, 1908762.
25 M. Rafiee, S. Chandra, H. Ahmed and S. J. McCormack, *Opt. Mater.*, 2019, **91**, 212–227.
26 H. Y. Huang, K. B. Cai, Y. R. Sie, K. Li, J. M. Yeh and C. T. Yuan, *Sol. RRL*, 2019, **3**, 1800347.
27 P. Moraitis, R. E. I. Schropp and W. G. J. H. M. van Sark, *Opt. Mater.*, 2018, **84**, 636–645.
28 O. M. ten Kate, K. W. Kramer and E. van der Kolk, *Sol. Energy Mater. Sol. Cells*, 2015, **140**, 115–120.
29 K. Wu, H. Li and V. I. Klimov, *Nat. Photonics*, 2018, **12**, 105–110.
30 Y. Zhou, H. Zhao, D. Ma and F. Rosei, *Chem. Soc. Rev.*, 2018, **47**, 5866–5890.
31 F. Meinardi, F. Bruni and S. Brovelli, *Nat. Rev. Mater.*, 2017, **2**, 17072.
32 M. G. Debije and P. P. C. Verbunt, *Adv. Energy Mater.*, 2012, **2**, 12–35.
33 Y. L. Li, X. Q. Zhang, Y. C. Zhang, R. Dong and C. K. Luscombe, *J. Polym. Sci., Part A: Polym. Chem.*, 2019, **57**, 201–215.
34 B. R. Sutherland, *Joule*, 2018, **2**, 203–204.
35 J. ter Schiphorst, M. L. M. K. H. Y. K. Cheng, M. van der Heijden, R. L. Hageman, E. L. Bugg, T. J. L. Wagenaar and M. G. Debije, *Energy Build.*, 2020, **207**, 109625.
36 G. Albano, T. Colli, L. Nucci, R. Charaf, T. Biver, A. Pucci and L. A. Aronica, *Dyes Pigm.*, 2020, **174**, 108100.
37 E. Bagherzadeh-Khajehmarjan, A. Nikniazi, B. Olyaeefar, S. Ahmadi-Kandjani and J. M. Nunzi, *Sol. Energy Mater. Sol. Cells*, 2019, **192**, 44–51.
38 M. R. Bergren, N. S. Makarov, K. Ramasamy, A. Jackson, R. Gughelmetti and H. McDaniel, *ACS Energy Lett.*, 2018, **3**, 520–525.
39 X. Luo, T. Ding, X. Liu, Y. Liu and K. Wu, *Nano Lett.*, 2019, **19**, 338–341.
40 F. Meinardi, S. Ehrenberg, L. Dhamo, F. Carulli, M. Mauri, F. Bruni, R. Simonutti, U. Kortshagen and S. Brovelli, *Nat. Photonics*, 2017, **11**, 177–185.
41 F. Meinardi, H. McDaniel, F. Carulli, A. Colombo, K. A. Velizhanin, N. S. Makarov, R. Simonutti, V. I. Klimov and S. Brovelli, *Nat. Nanotechnol.*, 2015, **10**, 878–885.
42 H.-J. Song, B. G. Jeong, J. Lim, D. C. Lee, W. K. Bae and V. I. Klimov, *Nano Lett.*, 2018, **18**, 395–404.
43 Y. You, X. Tong, W. Wang, J. Sun, P. Yu, H. Ji, X. Niu and Z. M. Wang, *Adv. Sci.*, 2019, **6**, 1801967.
44 R. Adhikari, K. Basu, Y. Zhou, F. Vetrone, D. Ma, S. Sun, F. Vidal, H. Zhao and F. Rosei, *J. Mater. Chem. A*, 2018, **6**, 6822–6829.
45 H. Zhao, Y. Zhou, D. Benetti, D. Ma and F. Rosei, *Nano Energy*, 2017, **37**, 214–223.
46 Y. Zhou, D. Benetti, Z. Fan, H. Zhao, D. Ma, A. O. Govorov, A. Vomiero and F. Rosei, *Adv. Energy Mater.*, 2016, **6**, 1501913.
47 A. Anand, M. L. Zaffalon, G. Gariano, A. Camellini, M. Gandini, R. Brescia, C. Capitani, F. Bruni, V. Pinchetti, M. Zavelani-Rossi, F. Meinardi, S. A. Crooker and S. Brovelli, *Adv. Funct. Mater.*, 2019, **30**, 1906629.
48 T. A. Cohen, T. J. Milstein, D. M. Kroupa, J. D. MacKenzie, C. K. Luscombe and D. R. Gamelin, *J. Mater. Chem. A*, 2019, **7**, 9279–9288.
49 I. Coropceanu and M. G. Bawendi, *Nano Lett.*, 2014, **14**, 4097–4101.
50 C. S. Erickson, L. R. Bradshaw, S. McDowall, J. D. Gilbertson, D. R. Gamelin and D. L. Patrick, *ACS Nano*, 2014, **8**, 3461–3467.
51 H. Zhao, R. Sun, Z. Wang, K. Fu, X. Hu and Y. Zhang, *Adv. Funct. Mater.*, 2019, **29**, 1902262.
52 X. Liu, B. Luo, J. Liu, D. Jing, D. Benetti and F. Rosei, *J. Mater. Chem. A*, 2020, **8**, 1787–1798.
53 R. Mazzaro and A. Vomiero, *Adv. Energy Mater.*, 2018, **8**, 1801903.
54 M. Wen, Z. X. Qin, W. H. Wang, J. C. Cui, R. Zhang, Q. M. Zhang, K. Li, J. H. Li, W. Yang and Y. Zhou, *Mol. Phys.*, 2020, DOI: 10.1080/00268976.2019.1710609.
55 C. J. Wang, H. X. Shi, M. Yang, Y. J. Yan, E. Z. Liu, Z. Ji and J. Fan, *Mater. Res. Bull.*, 2020, **124**, 110730.
56 J. Z. Guo, H. Li, L. T. Ling, G. Li, R. Cheng, X. Lu, A. Q. Xie, Q. Li, C. F. Wang and S. Chen, *ACS Sustainable Chem. Eng.*, 2020, **8**, 1566–1572.
57 Z. Rahmani and M. Ghaemy, *Opt. Mater.*, 2019, **97**, 109356.
58 M. Muthukumaran, G. Dhinagaran, V. Narayanan, T. Raju and K. Venkatachalam, *J. Indian Chem. Soc.*, 2019, **96**, 78–80.
59 S. S. Jing, Y. S. Zhao, R. C. Sun, L. X. Zhong and X. W. Peng, *ACS Sustainable Chem. Eng.*, 2019, **7**, 7833–7843.
60 H. Huang, C. G. Li, Z. Shi and S. H. Feng, *Chem. J. Chin. Univ.*, 2019, **40**, 1579–1585.
61 B. T. Hoan, P. D. Tam and V. H. Pham, *J. Nanotechnol.*, 2019, 2852816.
62 Y. Fu, G. Y. Gao and J. F. Zhi, *J. Mater. Chem. B*, 2019, **7**, 1494–1502.
63 T. V. de Medeiros, J. Manioudakis, F. Noun, J. R. Macairan, F. Victoria and R. Naccache, *J. Mater. Chem. C*, 2019, **7**, 7175–7195.
64 R. Tabaraki and N. Sadeghinejad, *Ecotoxicol. Environ. Saf.*, 2018, **153**, 101–106.
65 M. Shamsipur, K. Molaei, F. Molaabasi, S. Hosseinkhani, N. Alizadeh, M. Alipour and S. Moassess, *Sens. Actuators, B*, 2018, **257**, 772–782.

66 V. Ramanan, S. H. Subray and P. Ramamurthy, *New J. Chem.*, 2018, **42**, 8933–8942.
67 X. Miao, D. Qu, D. X. Yang, B. Nie, Y. K. Zhao, H. Y. Fan and Z. C. Sun, *Adv. Mater.*, 2018, **30**, 1704740.
68 H. Y. Li, Y. Xu, J. Ding, L. Zhao, T. Y. Zhou, H. Ding, Y. H. Chen and L. Ding, *Microchim. Acta*, 2018, **185**, 104.
69 K. Jiang, Y. H. Wang, X. L. Gao, C. Z. Cai and H. W. Lin, *Angew. Chem., Int. Ed.*, 2018, **57**, 6216–6220.
70 H. Ding, J. S. Wei, P. Zhang, Z. Y. Zhou, Q. Y. Gao and H. M. Xiong, *Small*, 2018, **14**, 1800612.
71 Q. Xiao, Y. Liang, F. W. Zhu, S. Y. Lu and S. Huang, *Microchim. Acta*, 2017, **184**, 2429–2438.
72 V. Roshni and O. Divya, *Curr. Sci.*, 2017, **112**, 385–390.
73 P. Namdari, B. Negahdari and A. Eatemadi, *Biomed. Pharmacother.*, 2017, **87**, 209–222.
74 Y. Q. Zhang, X. Y. Liu, Y. Fan, X. Y. Guo, L. Zhou, Y. Lv and J. Lin, *Nanoscale*, 2016, **8**, 15281–15287.
75 Y. R. Yan, Q. T. Huang, C. Wei, S. R. Hu, H. Q. Zhang, W. X. Zhang, W. Z. Yang, P. H. Dong, M. L. Zhu and Z. M. Wang, *RSC Adv.*, 2016, **6**, 115317–115325.
76 Z. F. Wang, J. F. Yu, X. Zhang, N. Li, B. Liu, Y. Y. Li, Y. H. Wang, W. X. Wang, Y. Z. Li, L. C. Zhang, S. Dissanayake, S. L. Suib and L. Y. Sun, *ACS Appl. Mater. Interfaces*, 2016, **8**, 1434–1439.
77 L. Wang, Y. D. Bi, J. Hou, H. Y. Li, Y. Xu, B. Wang, H. Ding and L. Ding, *Talanta*, 2016, **160**, 268–275.
78 C. Y. Yu, T. T. Xuan, Y. W. Chen, Z. J. Zhao, Z. Sun and H. L. Li, *J. Mater. Chem. C*, 2015, **3**, 9514–9518.
79 V. Chaudhary and A. K. Bhowmick, *Korean J. Chem. Eng.*, 2015, **32**, 1707–1711.
80 Y. Kim, H. Namgung, Y. Kim, G. Jang and T. S. Lee, *Sci. Adv. Mater.*, 2014, **6**, 2440–2444.
81 J. H. Deng, Q. J. Lu, N. X. Mi, H. T. Li, M. L. Liu, M. C. Xu, L. Tan, Q. J. Xie, Y. Y. Zhang and S. Z. Yao, *Chem. – Eur. J.*, 2014, **20**, 4993–4999.
82 D. L. Xiao, D. H. Yuan, H. He and M. M. Gao, *J. Lumin.*, 2013, **140**, 120–125.
83 H. Y. Wu, C. C. Mi, H. Q. Huang, B. F. Han, J. Li and S. K. Xu, *J. Lumin.*, 2012, **132**, 1603–1607.
84 W. B. Lu, X. Y. Qin, S. Liu, G. H. Chang, Y. W. Zhang, Y. L. Luo, A. M. Asiri, A. O. Al-Youbi and X. P. Sun, *Anal. Chem.*, 2012, **84**, 5351–5357.
85 S. Anwar, H. Ding, M. Xu, X. Hu, Z. Li, J. Wang, L. Liu, L. Jiang, D. Wang, C. Dong, M. Yan, Q. Wang and H. Bi, *ACS Appl. Bio Mater.*, 2019, **2**, 2317–2338.
86 S. N. Qu, D. Zhou, D. Li, W. Y. Ji, P. T. Jing, D. Han, L. Liu, H. B. Zeng and D. Z. Shen, *Adv. Mater.*, 2016, **28**, 3516–3521.
87 K. Hola, M. Sudolska, S. Kalytchuk, D. Nachtigallova, A. L. Rogach, M. Otyepka and R. Zboril, *ACS Nano*, 2017, **11**, 12402–12410.
88 F. L. Yuan, T. Yuan, L. Z. Sui, Z. B. Wang, Z. F. Xi, Y. C. Li, X. H. Li, L. Z. Fan, Z. A. Tan, A. M. Chen, M. X. Jin and S. H. Yang, *Nat. Commun.*, 2018, **9**, 2249.
89 T. K. Mondal, A. Gupta, B. K. Shaw, S. Mondal, U. K. Ghorai and S. K. Saha, *RSC Adv.*, 2016, **6**, 59927–59934.
90 M. Raeisossadati, N. R. Moheimani and D. Parlevliet, *Algal Res.*, 2020, **45**, 101771.
91 R. B. Ren, Z. Y. Zhang, P. H. Zhao, J. T. Shi, K. C. Han, Z. Q. Yang, D. X. Gao and F. Bi, *J. Dispersion Sci. Technol.*, 2019, **40**, 627–633.
92 M. Raeisossadati, N. R. Moheimani and D. Parlevliet, *Bioresour. Technol.*, 2019, **291**, 121801.
93 B. C. M. Martindale, G. A. M. Hutton, C. A. Caputo and E. Reisner, *J. Am. Chem. Soc.*, 2015, **137**, 6018–6025.
94 M. Shamsipur, A. Barati, A. A. Taherpour and M. Jamshidi, *J. Phys. Chem. Lett.*, 2018, **9**, 4189–4198.
95 M. Y. Xue, J. J. Zhao, Z. H. Zhan, S. L. Zhao, C. Q. Lan, F. G. Ye and H. Liang, *Nanoscale*, 2018, **10**, 18124–18130.
96 D. Zhou, P. T. Jing, Y. Wang, Y. C. Zhai, D. Li, Y. Xiong, A. V. Baranov, S. N. Qu and A. L. Rogach, *Nanoscale Horiz.*, 2019, **4**, 388–395.
97 W. J. Liu, C. Li, X. B. Sun, W. Pan, G. F. Yu and J. P. Wang, *Nanotechnology*, 2017, **28**, 485705.
98 Y. Y. Yao, G. Gedda, W. M. Girma, C. L. Yen, Y. C. Ling and J. Y. Chang, *ACS Appl. Mater. Interfaces*, 2017, **9**, 13887–13899.
99 M. Y. Si, J. Zhang, Y. Y. He, Z. Q. Yang, X. Yan, M. R. Liu, S. N. Zhuo, S. Wang, X. B. Min, C. J. Gao, L. Y. Chai and Y. Shi, *Green Chem.*, 2018, **20**, 3414–3419.
100 H. G. Huang, S. W. Yang, Q. T. Li, Y. C. Yang, G. Wang, X. F. You, B. H. Mao, H. S. Wang, Y. Ma, P. He, Z. Liu, G. Q. Ding and X. M. Xie, *Langmuir*, 2018, **34**, 250–258.
101 M. Q. He, X. R. Guo, J. Z. Huang, H. H. Shen, Q. Zeng and L. S. Wang, *Carbon*, 2018, **140**, 508–520.
102 H. R. Jia, Z. B. Wang, T. Yuan, F. L. Yuan, X. H. Li, Y. C. Li, Z. A. Tan, L. Z. Fan and S. H. Yang, *Adv. Sci.*, 2019, **6**, 1900397.
103 F. Yuan, Y. K. Wang, G. Sharma, Y. Dong, X. Zheng, P. Li, A. Johnston, G. Bappi, J. Z. Fan, H. Kung, B. Chen, M. I. Saidaminov, K. Singh, O. Voznyy, O. M. Bakr, Z. H. Lu and E. H. Sargent, *Nat. Photonics*, 2019, **14**, 171–176.
104 J. Zhang, L. Yang, Y. Yuan, J. Jiang and S. H. Yu, *Chem. Mater.*, 2016, **28**, 4367–4374.
105 M. J. Talite, H.-Y. Huang, Y.-H. Wu, P. G. Sena, K.-B. Cai, T.-N. Lin, J.-L. Shen, W.-C. Chou and C.-T. Yuan, *ACS Appl. Mater. Interfaces*, 2018, **10**, 34184–34192.
106 Y. Li, P. Miao, W. Zhou, X. Gong and X. Zhao, *J. Mater. Chem. A*, 2017, **5**, 21452–21459.
107 D. Qu, M. Zheng, L. Zhang, H. Zhao, Z. Xie, X. Jing, R. E. Haddad, H. Fan and Z. Sun, *Sci. Rep.*, 2014, **4**, 5294.
108 H. Ding, S. B. Yu, J. S. Wei and H. M. Xiong, *ACS Nano*, 2016, **10**, 484–491.
109 B. Yuan, S. Y. Guan, X. M. Sun, X. M. Li, H. B. Zeng, Z. Xie, P. Chen and S. Y. Zhou, *ACS Appl. Mater. Interfaces*, 2018, **10**, 16005–16014.
110 B. Ju, H. Nie, Z. Liu, H. Xu, M. Li, C. Wu, H. Wang and S. X. A. Zhang, *Nanoscale*, 2017, **9**, 13326–13333.
111 B. Ju, H. Nie, X. G. Zhang, Q. Chen, X. Guo, Z. Xing, M. Li and S. X. A. Zhang, *ACS Appl. Nano Mater.*, 2018, **1**, 6131–6138.

112 Z. H. Wen and X. B. Yin, *RSC Adv.*, 2016, **6**, 27829–27835.
113 D. Chen, X. Chen, H. Gao and J. Zhong, *RSC Adv.*, 2018, **8**, 29855–29861.
114 L. Bao, C. Liu, Z. L. Zhang and D. W. Pang, *Adv. Mater.*, 2015, **27**, 1663–1667.
115 S. Lu, L. Sui, J. Liu, S. Zhu, A. Chen, M. Jin and B. Yang, *Adv. Mater.*, 2017, **29**, 1603443.
116 D. Li, P. T. Jing, L. H. Sun, Y. An, X. Y. Shan, X. H. Lu, D. Zhou, D. Han, D. Z. Shen, Y. C. Zhai, S. N. Qu, R. Zbořil and A. L. Rogach, *Adv. Mater.*, 2018, **30**, 1705913.
117 X. X. Shi, H. M. Meng, Y. Q. Sun, L. B. Qu, Y. H. Lin, Z. H. Li and D. Du, *Small*, 2019, **15**, 1901507.
118 Y. Choi, B. Kang, J. Lee, S. Kim, G. T. Kim, H. Kang, B. R. Lee, H. Kim, S. H. Shim, G. Lee, O. H. Kwon and B. S. Kim, *Chem. Mater.*, 2016, **28**, 6840–6847.
119 H. Zhao, *J. Lumin.*, 2019, **211**, 150–156.
120 S. K. E. Hill, R. Connell, C. Peterson, J. Hollinger, M. A. Hillmyer, U. Kortshagen and V. E. Ferry, *ACS Photonics*, 2019, **6**, 170–180.
121 H. B. Li, K. F. Wu, J. Lim, H. J. Song and V. I. Klimov, *Nat. Energy*, 2016, **1**, 16157.
122 F. Khan and J. H. Kim, *ACS Photonics*, 2018, **5**, 4637–4643.
123 F. L. Yuan, Z. B. Wang, X. H. Li, Y. C. Li, Z. A. Tan, L. Z. Fan and S. H. Yang, *Adv. Mater.*, 2017, **29**, 1604436.
124 J. M. Delgado-Sanchez, *Sol. Energy Mater. Sol. Cells*, 2019, **202**, 110134.
125 J. Y. Wang, Y. C. Yuan, H. Zhu, T. Cai, Y. Fang and O. Chen, *Nano Energy*, 2020, **67**, 4.
126 H. G. Zhao, G. J. Liu and G. T. Han, *Nanoscale Adv.*, 2019, **1**, 4888–4894.
127 F. Mateen, M. Ali, S. Y. Lee, S. H. Jeong, M. J. Ko and S. K. Hong, *Sol. Energy*, 2019, **190**, 488–494.
128 Z. X. Han, Y. Q. Ni, J. K. Ren, W. F. Zhang, Y. F. Wang, Z. Xie, S. Y. Zhou and S. F. Yu, *Nanoscale*, 2019, **11**, 11577–11583.
129 Z. F. Wang, F. L. Yuan, X. H. Li, Y. C. Li, H. Z. Zhong, L. Z. Fan and S. H. Yang, *Adv. Mater.*, 2017, **29**, 1702910.
130 Z. J. Wang, X. J. Zhao, Z. Z. Guo, P. Miao and X. Gong, *Org. Electron.*, 2018, **62**, 284–289.
131 H. G. Zhao, D. Benetti, X. Tong, H. Zhang, Y. F. Zhou, G. J. Liu, D. L. Ma, S. H. Sun, Z. M. M. Wang, Y. Q. Wang and F. Rosei, *Nano Energy*, 2018, **50**, 756–765.
132 W. W. Ma, W. J. Li, R. Y. Liu, M. Y. Cao, X. J. Zhao and X. Gong, *Chem. Commun.*, 2019, **55**, 7486–7489.
133 F. Mateen, M. Ali, H. Oh and S. K. Hong, *Sol. Energy*, 2019, **178**, 48–55.
134 M. J. Talite, H. Y. Huang, K. B. Cai, K. C. C. Co, P. A. C. Santoso, S. H. Chang, W. C. Chou and C. T. Yuan, *J. Phys. Chem. Lett.*, 2020, **11**, 567–573.
135 W. Ma, W. Li, M. Cao, R. Liu, X. Zhao and X. Gong, *Org. Electron.*, 2019, **73**, 226–230.
136 Y. Wang and X. Gong, *J. Mater. Chem. A*, 2017, **5**, 3759–3773.
137 M. Zhu, Y. Li, S. Tian, Y. Xie, X. Zhao and X. Gong, *J. Colloid Interface Sci.*, 2019, **534**, 509–517.
138 F. Meinardi, A. Colombo, K. A. Velizhanin, R. Simonutti, M. Lorenzon, L. Beverina, R. Viswanatha, V. I. Klimov and S. Brovelli, *Nat. Photonics*, 2014, **8**, 392–399.
139 G. Liu, R. Mazzaro, Y. Wang, H. Zhao and A. Vomiero, *Nano Energy*, 2019, **60**, 119–126.
140 G. Liu, R. Mazzaro, C. Sun, Y. Zhang, Y. Wang, H. Zhao, G. Han and A. Vomiero, *Nano Energy*, 2020, **70**, 104470.
141 H. Zhao, D. Benetti, L. Jin, Y. Zhou, F. Rosei and A. Vomiero, *Small*, 2016, **12**, 5354–5365.
142 M. J. Currie, J. K. Mapel, T. D. Heidel, S. Goffri and M. A. Baldo, *Science*, 2008, **321**, 226–228.
143 L. H. Slooff, E. E. Bende, A. R. Burgers, T. Budel, M. Pravettoni, R. P. Kenny, E. D. Dunlop and A. Büchtemann, *Phys. Status Solidi RRL*, 2008, **2**, 257–259.
144 L. Zdražil, S. Kalytchuk, K. Holá, M. Petr, O. Zmeškal, Š. Kment, A. L. Rogach and R. Zbořil, *Nanoscale*, 2020, **12**, 6664–6672.
145 Scientific Polymer Products, Inc., Refractive Index of Polymers by Index, https://scientificpolymer.com/technical-library/refractive-index-of-polymers-by-index/.
146 S. Sadeghi, R. Melikov, H. Bahmani Jalali, O. Karatum, S. B. Srivastava, D. Conkar, E. N. Firat-Karalar and S. Nizamoglu, *ACS Appl. Mater. Interfaces*, 2019, **11**, 8710–8716.
147 A. H. Khan, V. Pinchetti, I. Tanghe, Z. Dang, B. Martín-García, Z. Hens, D. Van Thourhout, P. Geiregat, S. Brovelli and I. Moreels, *Chem. Mater.*, 2019, **31**, 1450–1459.
148 C. Zhou, H. Lin, Y. Tian, Z. Yuan, R. Clark, B. Chen, L. J. van de Burgt, J. C. Wang, Y. Zhou, K. Hanson, Q. J. Meisner, J. Neu, T. Besara, T. Siegrist, E. Lambers, P. Djurovich and B. Ma, *Chem. Sci.*, 2018, **9**, 586–593.
149 W. van Sark, P. Moraitis, C. Aalberts, M. Drent, T. Grasso, Y. L'Ortije, M. Visschers, M. Westra, R. Plas and W. Planje, *Sol. RRL*, 2017, **1**, 1600015.
150 C. Corrado, S. W. Leow, M. Osborn, I. Carbone, K. Hellier, M. Short, G. Alers and S. A. Carter, *J. Renewable Sustainable Energy*, 2016, **8**, 043502.
151 M. Kanellis, M. M. de Jong, L. Slooff and M. G. Debije, *Renewable Energy*, 2017, **103**, 647–652.
152 D. Cambie, F. Zhao, V. Hessel, M. G. Debije and T. Noel, *Angew. Chem., Int. Ed.*, 2017, **56**, 1050–1054.
153 G. Liu, B. Sun, H. Li, Y. Wang and H. Zhao, *J. Mater. Chem. A*, 2019, **7**, 18529–18537.